AD-A154 915 2-D SIMULATIONS OF THE NRL (NAVAL RESEARCH LABORATORY) LASER EXPERIMENT(U) NAVAL RESEARCH LAB WASHINGTON DC J G LYON 08 MAY 85 NRL-MR-5491 1/1

UNCLASSIFIED F/G 20/5 NL

END

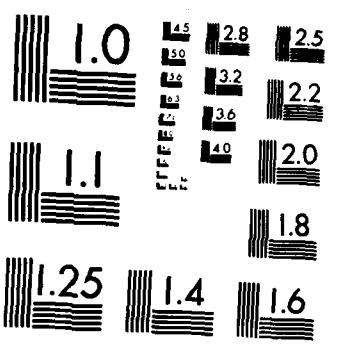

(2)

NRL Memorandum Report 5491

2-D Simulations of the NRL Laser Experiment

J. G. LYON

Geophysical and Plasma Dynamics Branch
Plasma Physics Division

May 8, 1985

This research was sponsored by the Defense Nuclear Agency under Subtask S99QMXBC, work unit 00102 and work unit title "Plasma Structure Evolution."

NAVAL RESEARCH LABORATORY
Washington, D.C.

SECURITY CLASSIFICATION OF THIS PAGE

REPORT DOCUMENTATION PAGE

1a REPORT SECURITY CLASSIFICATION UNCLASSIFIED	1b RESTRICTIVE MARKINGS
2a SECURITY CLASSIFICATION AUTHORITY	3 DISTRIBUTION/AVAILABILITY OF REPORT
2b DECLASSIFICATION/DOWNGRADING SCHEDULE	Approved for public release; distribution unlimited.
4 PERFORMING ORGANIZATION REPORT NUMBER(S) NRL Memorandum Report 5491	5 MONITORING ORGANIZATION REPORT NUMBER(S)
6a NAME OF PERFORMING ORGANIZATION Naval Research Laboratory 6b OFFICE SYMBOL (If applicable) Code 4780	7a NAME OF MONITORING ORGANIZATION
6c ADDRESS (City, State, and ZIP Code) Washington, DC 20375-5000	7b ADDRESS (City, State, and ZIP Code)
8a NAME OF FUNDING/SPONSORING ORGANIZATION Defense Nuclear Agency 8b OFFICE SYMBOL (If applicable) RAAE	9 PROCUREMENT INSTRUMENT IDENTIFICATION NUMBER
8c ADDRESS (City, State, and ZIP Code) Washington, DC 20305	10 SOURCE OF FUNDING NUMBERS PROGRAM ELEMENT NO: 62715H; PROJECT NO:; TASK NO:; WORK UNIT ACCESSION NO: DN580-072

11 TITLE (Include Security Classification)
2-D Simulations of the NRL Laser Experiment

12 PERSONAL AUTHOR(S)
Lyon, J.G.

13a TYPE OF REPORT	13b TIME COVERED	14 DATE OF REPORT (Year, Month, Day)	15 PAGE COUNT
Interim	FROM 10/83 TO 10/84	1985 May 8	38

16 SUPPLEMENTARY NOTATION This research was sponsored by the Defense Nuclear Agency under Subtask S99QMXBC, work unit 00102 and work unit title "Plasma Structure Evolution."

17 COSATI CODES			18 SUBJECT TERMS (Continue on reverse if necessary and identify by block number)
FIELD	GROUP	SUB-GROUP	Gas-dynamics, Laser, Blast waves, Numerical simulation, Stability,

19 ABSTRACT (Continue on reverse if necessary and identify by block number)

Two-dimensional gas-dynamic simulations of the NRL laser experiment have been performed to study the formation of aneurysms in the blast wave and to study the formation of structure internal to the blast front itself. In one set of simulations the debris shell was perturbed sinusoidally in mass and position and also perturbed to mimic the action of a slow jet of material leaving the target at slower speeds than the bulk of the debris. In all cases the blast wave remained stable to any aneurysm-like instability. Internal structure, however, was quite easily produced and grew as a function of time. In the other set of simulations the effect of a pre-heated channel upon the propagation of the blast wave was examined. Bulges in the blast wave shock front were produced in these simulations that could be the beginning of the aneurysm phenomenon, but the pre-heated channel by itself appears to be insufficient to produce the observed aneurysms.

20 DISTRIBUTION/AVAILABILITY OF ABSTRACT	21 ABSTRACT SECURITY CLASSIFICATION	
☒ UNCLASSIFIED/UNLIMITED ☐ SAME AS RPT ☐ DTIC USERS	UNCLASSIFIED	
22a NAME OF RESPONSIBLE INDIVIDUAL J. D. Huba	22b TELEPHONE (Include Area Code) (202) 767-3630	22c OFFICE SYMBOL Code 4780

DD FORM 1473, 84 MAR 83 APR edition may be used until exhausted
All other editions are obsolete

SECURITY CLASSIFICATION OF THIS PAGE

CONTENTS

2-D SIMULATIONS OF THE NRL LASER EXPERIMENT

I. Introduction

We present the results of two sets of simulations of the DNA/NRL laser experiment using a two-dimensional gas-dynamic code. The set of simulations discussed were prompted by the structure seen in the expanding shock front in recent experiments (*e.g.* Stamper *et al.*, 1984). These experiments were run in the high ambient pressure, hydrodynamic regime. In general these experiments show the formation of expanding bubbles or aneurysms on the shock front. Data from the experiment show that the shock has the character of a self-similar blast wave; such a blast wave is generally stable. The question, then, that these simulations attempt to answer is whether it is possible to perturb the initial conditions sufficiently in the ablated target material or in the ambient surroundings to give rise to the aneurysms seen in the experiment. In the first set of simulations we perturb or deform the distribution of the ablated target debris in order to discover whether the resulting blast wave becomes unstable to an aneurysm-like deformation. In the second set of simulations, we study how an inhomogeneity in the ambient initial conditions – in this case a pre-heated channel – might affect the propagation of the blast wave.

A second question can be studied with these simulations that is of interest for the seeding of late-time structure in a HANE. It is predicted theoretically (*e.g.*, Richtmeyer, 1960) and observed experimentally (Andronov *et al.*, 1976) that the contact surface between two media can be made Rayleigh-Taylor unstable by the passage of a shock across the boundary. Such a process can occur in the debris-air interface of a HANE and might be responsible for phenomena seen at later times. Thus, in these simulations we were also interested in the question of whether the applied perturbation in the debris shell damped out as the shocked region grew, or whether the perturbation grew as a function of time.

Manuscript approved October 17, 1984.

II. Perturbed Debris Shells

In this section, the ambient material into which the debris moves is assumed to be uniform, and it is the debris shell which is given perturbations of various forms to see whether any of these perturbations grow in time. Two different types of perturbations are discussed below. The first type is what is usually meant by a perturbation, a small change in a uniform state. Here both the shell position and mass distribution were given such small variations. The second type of perturbation follows a suggestion from C. Longmire that a slower jet of material coming behind the main debris shell may be responsible for the aneurysms. The results of simulating such jets are given below. We use the term perturbation for these simulations loosely, since the change in the initial conditions here is quite large in magnitude.

All the calculations discussed in this section were made using a cylindrical geometry. A spherical geometry is more in keeping with the general symmetry of the laser experiment. To test the general stability of debris shells we prefer not to choose a special coordinate direction as we would if we used the polar angle in a spherical coordinate system. The other angular coordinate in the spherical case is the azimuthal one. This leads to reasonable results only if the polar angle subtended is quite small and there is no structure in that direction. Neither of these conditions appears to be well satisfied for the laser experiment. Thus, cylindrical symmetry was chosen as a compromise that could be used over large angular extents and still contain the effects of the radial divergence terms in the equations. The following set of equations were solved:

Continuity

$$\frac{\partial \rho}{\partial t} = -\frac{1}{r}\frac{\partial}{\partial r} r\rho v_r - \frac{1}{r}\frac{\partial}{\partial \theta}\rho v_\theta \qquad (1.a)$$

Momentum

$$\frac{\partial p_r}{\partial t} = -\frac{1}{r}\frac{\partial}{\partial r} r(p_r v_r + P) - \frac{1}{r}\frac{\partial}{\partial \theta} p_\theta v_r + \frac{P}{r} \qquad (1.b)$$

$$\frac{\partial p_\theta}{\partial t} = -\frac{1}{r}\frac{\partial}{\partial r} r p_r v_\theta - \frac{1}{r}\frac{\partial}{\partial \theta}(p_\theta v_\theta + P) \qquad (1.c)$$

Energy

$$\frac{\partial E}{\partial t} = -\frac{1}{r}\frac{\partial}{\partial r} r v_r (E + P) - \frac{1}{r}\frac{\partial}{\partial \theta} v_\theta (E + P) \qquad (1.d)$$

where

$$E \equiv \frac{1}{2}\rho({v_\theta}^2 + {v_r}^2) + \frac{P}{\gamma - 1}$$

$$p_\theta \equiv \rho v_\theta$$

$$p_r \equiv \rho v_r$$

$$\gamma \equiv \text{ratio of specific heats}$$

The equations were solved in conservation form using an extension of the partial donor cell method, PDM (Hain 1978, Lyon, 1984). Eighth order centered spatial differencing and a second order time integration scheme (modified Euler) were employed. The numerical grid was 40×40 cells.

The grid was continuously adapted in the r direction during the calculation, while the θ grid was fixed. The endpoints of the mesh in the radial direction were moved to keep all structure on the grid. The interior mesh points were spaced to provide resolution in the regions of steep gradients. This was done by minimizing the integral,

$$\int_{r_{min}}^{r_{max}} dr \int_{\theta_{min}}^{\theta_{max}} \left(w(r,\theta)\frac{\partial r}{\partial i} + \lambda \left(\frac{\partial i}{\partial r}\right)^2 \right) \tag{2}$$

at each time step. The radial coordinate, r, is assumed to be a function of the mesh coordinate, i. The second term in the integrand is a smoothness measure – the smaller the integral the smoother the mapping of r to i. The first term weights i to regions where w is large. In these calculations the weight function,

$$w(r,\theta) = \left(\frac{1}{\rho}\frac{\partial \rho}{\partial r}\right)^2, \tag{3}$$

was used. This attempts to concentrate points in the regions of large density gradients. The quantity, λ, is an adjustable parameter used to provide control over the balance between the two terms. For the series of runs discussed here λ was adjusted so that a maximum grid compression about three times that of uniform spacing occurred in the debris shell.

The initial conditions were designed to mimic shot number 13261 in the NRL laser experiment. This particular shot shows a single clearly defined aneurysm (Stamper *et al.*, 1984). The ambient gas pressure was 5 Torr with an ambient mean molecular weight about equal to that of the aluminum target. The debris velocity and mass ablated for the shot energy of 38 J were estimated from the scaling relations given by Ripin (1983). The debris velocity used was 575 km/sec. The shell width was taken to be 4 ns times 575 km/sec, or .23 cm. The shell was initially centered at 0.2 cm from the target, and it was assumed that there was

no ambient material within the shell's maximum radius. The mass ablated was estimated as .23 μg, which gave an estimated shell density of 7×10^{-6} gm/cm^3. This is an estimate of the shell density for the spherical case, but was used for these cylindrical simulations.

A. Perturbed Shells

Two types of perturbations were applied to the initial debris shell. In the first, the position of the shell was given a small sinusoidal ripple in the θ direction amounting to about 5% of the thickness of the shell. In the second, the shell position was unperturbed but the mass density within the shell was given a sinusoidal perturbation. In all cases no aneurysms were observed to form and any disturbance of the position of the outgoing shock quickly damped out.

The case of a 10% sinusoidal mass perturbation is typical. Figure 1 shows the density contours in the simualtion at two different times. In the first, Figure 1.a, 2.58 ns after the beginning of the calculation, we can see a double shock structure where the debris shell has interacted with the ambient gas. One shock is propagating outward into the ambient gas, the other inward through the debris shell. There is also a contact discontinuity separating the ambient from debris material. It is not apparent in the density plot because, by coincidence, the initial shell density and ambient density were the same. Figure 1.b shows the density about 3 ns later. The outer shock shows a slight bulge in the region of enhanced density – the center of the plot. This bulge quickly damps out, however, as seen in Figure 1.c. This figure shows the density some 6.5 ns later. The blast wave front now appears to be very uniform; the initial bulge has disappeared. In all the runs performed with these types of simulations the blast wave front was very stable to anything resembling an aneurysm.

While these runs gave stable blast waves there was a considerable amount of internal structure in the region of the contact surface between the debris material and the ambient gas. The developing irregularities can be seen in Figure 1, but it is easier to see them in Figure 2 which gives a contour plot of the temperature. Figure 2.a shows the temperature at about 6 ns into the calculation. The two shock fronts are apparent, and also apparent is a rippling of the contact surface region in between the two. Figure 2.b gives the temperature 6 ns later. A very large and growing distortion can be seen now in this same region. The rate of growth appears to be consistent with Richtmeyer's (1960) theory which predicts linear rather than exponential growth. Thus, a cylindrical or spherical geometry probably does not severely affect this mechanism. Irregularities in the debris shell can cause large irregularities in the internal structure of the blast wave bubble.

B. Slow Jets

These simulations were intended to test the idea that aneurysms could be formed by a jet of material leaving the target at a slower speed than the rest of the ejected material. When the shock wave produced by the initial material has slowed sufficiently, the slower material can overtake it and go on ahead producing an aneurysm-like protuberance of the blast wave surface. In these runs, the middle 10 cells of the calculation in the θ direction were given an enhanced density and a decreased velocity. The densities and velocities were chosen so that the "jet" region always had a higher momentum and energy than the rest of the shell. With this particular set of initial conditions, the bulk of the shell should move more quickly than the "jet" until enough mass is swept up for the blast wave solution to be set up. Thereafter, the higher energy in the "jet" should allow it to overtake the rest of the shell and proceed ahead. If there were no interaction between the two regions of the shell, at late times both would follow a blast wave solution with differing proportionality constants. This would imply that if this mechanism were responsible for aneurysms, the aneurysms would be self-similar structures on the surface of the blast wave. However, there clearly is strong coupling between the two regions, and it is the purpose of these calculations to determine whether that interaction helps or hinders the running ahead of the "jet".

Figure 3 shows the density evolution of a "small" jet. In this run, the density enhancement was $\delta\rho/\rho$ = 0.4 and the velocity decrease was $\delta v/v$ = -0.1. The increase in jet energy was thus $\approx$ 20%. In Figure 3.a, 2.6 ns after the start of the calculation, the enhanced density jet can be seen lagging slightly behind the the rest of the shell. In Figure 3.b, 3 ns later, the shock in front of the increased density region has caught up with the rest of the shell. The increased density is still apparent in the contours at this time. Figure 3.c shows the density at a very much later time, 39 ns. There is a slight irregularity in the shock front, but the jet region now lags *behind* the rest of the shell. Also the density of the shell has become much more uniform. It is difficult to pick out an increased density region in the θ driection, except very far inward from the shock. The transition from Figure 3.b to 3.c is a smooth one. In intermediate times the shock front in the jet region does run slightly ahead of the rest of the shell, but the major evolution seems to be a decrease in the density non-uniformity behind the shock in the θ dizection.

A higher density jet was also simulated as shown in Figure 4. Here $\delta\rho/\rho$ = 1.0 and $\delta v/v$ = -0.1. Thus, the energy within the shell is almost twice that of the rest of the shell. On the assumption that both regions follow their own blast wave solutions, this jet should run ahead of the rest of tha shell by about 15% of the shock radius. Figure 4.a shows the density very early in the calculation. The jet is already forging slightly ahead of the rest of the debris. In figures 4.b and 4.c at times 6.1 and 13.4 ns, respectively, the process continues. Note, however, that the

density irregularity behind the shock is strongly decreasing. Figure 4.c is about the peak of the advance of the jet over the rest of the material. The final figure 4.d shows the density at 41.4 ns. Here, the jet area lags behind the rest of the shell. Note also the density clumps behind the shock. The strange behavior of the flanks running ahead of the jet is almost certainly due to the periodic boundary conditions used in the θ direction. As the jet moves on ahead of the rest of the shell the shock wave in front of it slows relative to the rest of the shell and also broadens. As this braodening reaches the boundaries, a cusp-like structure is formed as the shock front and its image meet at an oblique angle at the boundary. This dumps shock energy in the region of the boundary, and the shock in the boundary region accelerates and overtakes the jet region. While such an analysis is not strictly valid for an expanding cylindrical shock, an explanation in terms of shock geometric optics can be found in Whitham (1974). Once the boundaries run ahead, they cause the same process to occur in the center of the grid , so that an oscillatory behavior is set up. This oscillation eventually damps. While interesting, the phenomenon does depend on the artificial boundary conditions used, and so is probably of little practical interest.

The density clumps observed behind the shock may be of considerable interest for a HANE, however. We note that tney begin to form even at $t = 6.1$ ns, far too early for the boundary conditions to affect the simulation. At later times the disturbance appears to cascade to a relatively short angular wavelength. In the final plot, Figure 4.d, the amplitude of these clumps is about 2 to 1 over the surroundings. The mechanism producing these clumps is not known, although the initial clump of to the side of the jet in Figure 4.b is apparently related to the vorticity set up by the differing velocities in the jet and the rest of the shell. It is quite possible that the large amplitude to which these clumps grow is due to the periodic boundary conditions. However, these small scale, high-amplitude irregularites could be a significant source of structure in at least some HANE's.

III. The Pre-Heated Channel

From the previous section it is apparent that an energy conserving explosion in the fluid regime is not spontaneously unstable to aneurysm-like modes. In fact, very special initial conditions with large amplitude irregularities must be formulated to produce anything resembling aneurysms. In this section we treat an alternative hypothesis; We assume that something creates a channel with a narrow angular extent in front of the blast wave. The conditions for the propagation of the shock within the channel are then different from those outside. The shock could then run faster within the channel than outside, leading to an aneurysm-like appearance. A weak piece of evidence in favor of this idea is that in the current series of laser shots, the aneurysm is usually single and roughly aligned with the laser or target normal axis. In fact, in one shot, where the target was tilted relative to the laser beam, two aneurysms were seen – one along the laser axis and the other along the target normal. We can only speculate about the possible cause of channel formation, but two possibilities are a "hot spot" in the laser beam and a beam of high energy ions produced by some microphysical process in the laser-target interaction.

There are a number of ways in which a pre-heated channel can affect the propagation of a blast wave. One possibility is that the shock wave runs faster through hotter material. Unfortunately, though the effect is in the proper direction to produce aneurysms, the magnitude is rather small. The speed of strong shocks is to lowest order independent of the temperature of the ambient gas. The first order correction to that speed, $\delta v/v$, is $\approx \gamma - 2/\gamma M^2$, where M is the Mach number of the shock in the ambient gas. The smaller the Mach number, the faster the shock runs for $\gamma < 2$. However, even if the gas is pre-heated to a temperature of about one eV, the corection still would appear to be only about 1%. A more sizeable effect is required. A second possibility is that if the gas is not in local thermodynamic equilibrium (LTE), the effective γ of the gas could change, thus affecting the shock speed. There is a relatively strong dependence of shock speed on $\gamma - R_{sh} \propto \gamma^{0.95}$ for $\gamma = 1.2$. While this is an interesting possibility, simulation of this case requires a very complex numerical model including chemical and transfer effects. Thus, we do not pursue this possibility here.

A third possibility is the one upon which we will concentrate in this section. A pre-heated channel can give rise to a lowered density ahead of the blast wave. The process is described as follows: Suppose a cylindrical channel is heated at some instant near the time of the laser pulse. There is a significant amount of time between that instant and the instant when the blast wave overruns the channel. During this time the heated gas is undergoing expansion away from the channel axis. If the material within the channel is much hotter than its surroundings, the density in the channel can become much lower than ambient. The rough time scale for such expansion is $t_c = \beta r_c/c_c$, where β is a constant on the order of unity, and r_c and c_c

are the initial radius and sound speed of the channel, respectively. For the ambient gas in ther laser experiments, assuming $r_c = 0.5$mm and $T_c = 5$ eV gives $t_c = \beta$ (100 ns). The time scale, t_c is thus roughly in the right range to be significant in the laser experiment. The quantity, β, is greater than one for a channel in which there is a step-function radial dependence of heating. The rarefaction wave which evacuates the center does not arrive there until t_c. A Gaussian-like radial dependence leads to faster results. Numerical experiments have shown that a significant lowering of density ($\approx 20\%$) at the center of the channel occurs at about 0.3 t_c. In this case t_c is defined by $\sigma_c/c_c(r = 0)$, where σ_c is the dispersion of the Gaussian and c_c is evaluated at thje center of the channel. A halving of the central density occurs at about $2t_c$. The density dependence of the blast speed upon density is not very strong. Still, assuming that the propagation of the shock down the channel is given by its own spherical blast wave dependence, *i.e.*

$$R_{sh} \propto \left(\frac{E_{bl}}{\rho_0}\right)^{0.2} t^{0.4}, \tag{4}$$

we can see that a 20% density reduction leads to about a 4% speed increase. That is not a large enough difference to produce aneurysms by itself, but it is large enough to make non-linear effects important.

Before going on to the simulations, it is worthwhile to discuss one further back-of-the-envelope argument. The formation of aneurysms occurs over a wide range of laser energies and ambient densitiies. As a rule of thumb, the lower the density or the higher the laser energy, the later does the aneurysm formation occur. We can see whether the pre-heated channel mechanism is consistent with such scaling by setting t_c equal to the time it takes the blast wave to reach a given distance from the origin. That is,

$$\left(\frac{E_{bl}}{\rho_0}\right)^{0.5} R_{sh}^{2.5} = \frac{k\theta_c R_{sh}}{\sqrt{E_{ch}}} \tag{5}$$

where the radius of the channel, r_c, is $\theta_c R_{sh}$ and k is a proportionality constant. As noted above the shock radius is proportional to $t^{0.4}$. The radius of the channel scales at a power closer to one. For very long times we might expect the channel expansion to go over into a cylindrical blast wave, where r_c would scale as $t^{0.5}$. In any event, the implication is that for all radii greater than the one found by solving (5), the channel should be well formed. Since we are only looking for scaling arguments, we solve (5) for a constant channel energy dropping most of the constants to obtain

$$R_{sh} \propto \left(\frac{E_{bl}}{\rho_0}\right)^{\frac{1}{3}} E_{ch}^{1/6} \theta_c^{2/3}. \tag{6}$$

This shows a fairly weak dependence on laser energy and ambient density, but he dependencies are in the right direction – higher laser energy and lower density ead to slower aneurysm formation. It might be reasonable to assume that the ›re-heating mechanism has an inverse square dependence from the target spot. Assuming $E_{ch} = E_0 R_0^2/R^2$, we get

$$R_{sh} \propto \left(\frac{E_{bl}}{\rho_0}\right) \theta_c^2 E_0^{-1} \tag{7}$$

which has a linear dependence on E_{bl} and ρ_0^{-1}. Once again, however, the dependencies are in the right direction to be consistent with the laser results. These arguments support the idea that the pre-heated channel is an explanation of the aneurysm phenomenon. The next sections deal with a numerical simulation of the effects of a pre-heated channel.

A. Simulations

A slightly different form of the code used in § II was used to simulate the pre-heated channel. While still two-dimensional, the variables were radius, r, from t' e target and the polar angle, θ. This is the most reasonable coordinate sytem to use for a 2-D simulation as long as there is a preferred axis along which the perturbation is expected to grow. Such is the case for the pre-heated channel. Secondly, while a cylindrically symmetric blast wave does not behave too differently from a spherical one, a slab symmetric channel (which would be the case for a cylindrical blast) acts quite differently from a cylindrically symmetric one. Since there seems to be a fairly sensitive trade-off between time scales associated with the blast wave and the channel, it is important in this case to use an accurate geometry.

The equations solved for these simulations were

Continuity

$$\frac{\partial \rho}{\partial t} = -\frac{1}{r^2}\frac{\partial}{\partial r} r^2 \rho v_r - \frac{1}{r \sin\theta}\frac{\partial}{\partial \theta} \sin\theta\, \rho v_\theta \tag{8.a}$$

Momentum

$$\frac{\partial p_r}{\partial t} = -\frac{1}{r^2}\frac{\partial}{\partial r} r^2 (p_r v_r + P) - \frac{1}{r \sin\theta}\frac{\partial}{\partial \theta} \sin\theta\, p_\theta v_r + \frac{2P}{r} \tag{8.b}$$

$$\frac{\partial p_\theta}{\partial t} = -\frac{1}{r^2}\frac{\partial}{\partial r} r^2 p_r v_\theta - \frac{1}{r \sin\theta}\frac{\partial}{\partial \theta} \sin\theta\, (p_\theta v_\theta + P) + \frac{P \cot\theta}{r} \tag{8.c}$$

(a)

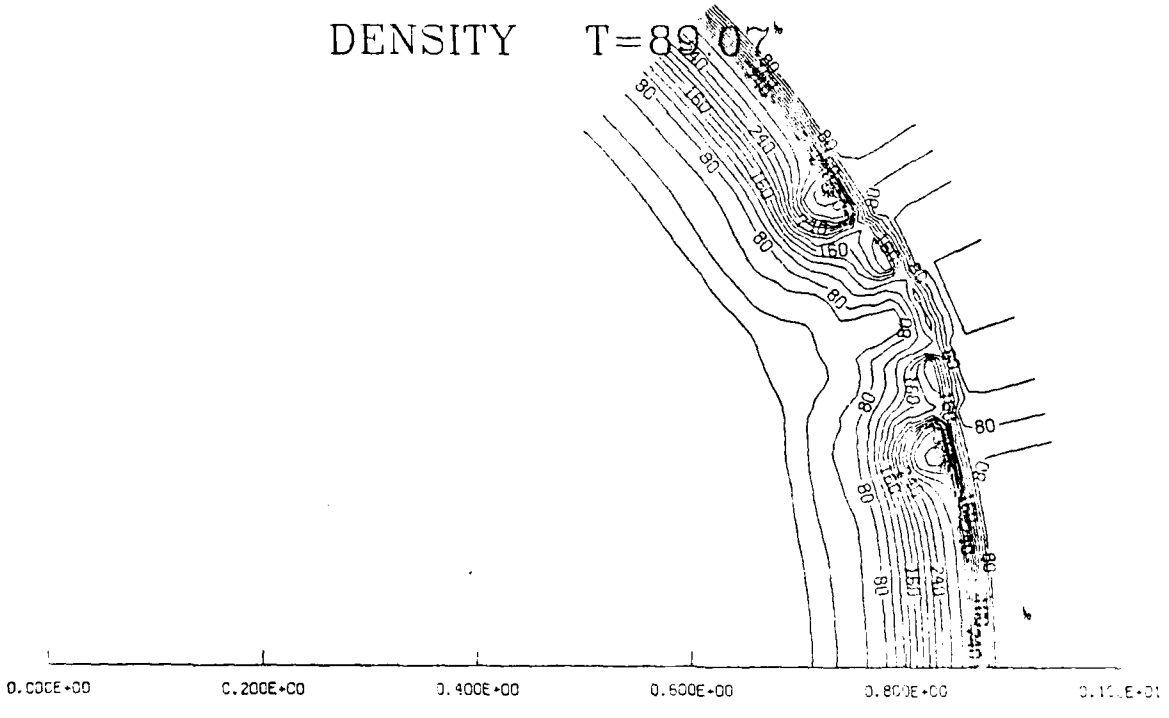

(b)

Fig. 6 — Density contours at selected times for a simulation with a constant initial channel temperature. The display format is similar to Figure 1. The contours are labeled in units of 1×10^{-7} gm/cm^3. The times displayed are: 6.a = 64.1 ns, and 6.b = 89.1 ns.

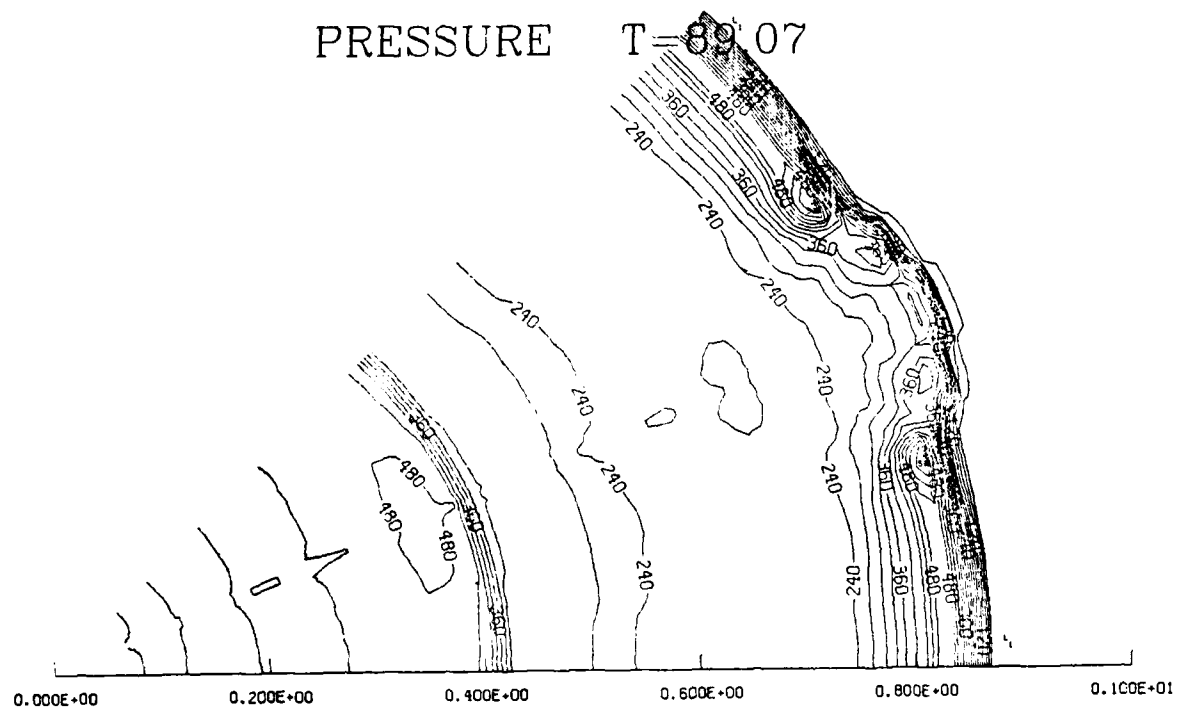

(c)

Fig. 5 (Cont'd) — Pressure contours at selected times for a simulation with a constant initial channel temperature. The display format is similar to Figure 1. The contours are labeled in units of 1×10^6 ergs/cm^3. The times displayed are: 5.a = 48.9 ns, 5.b = 64.1 ns, and 5.c = 89.1 ns.

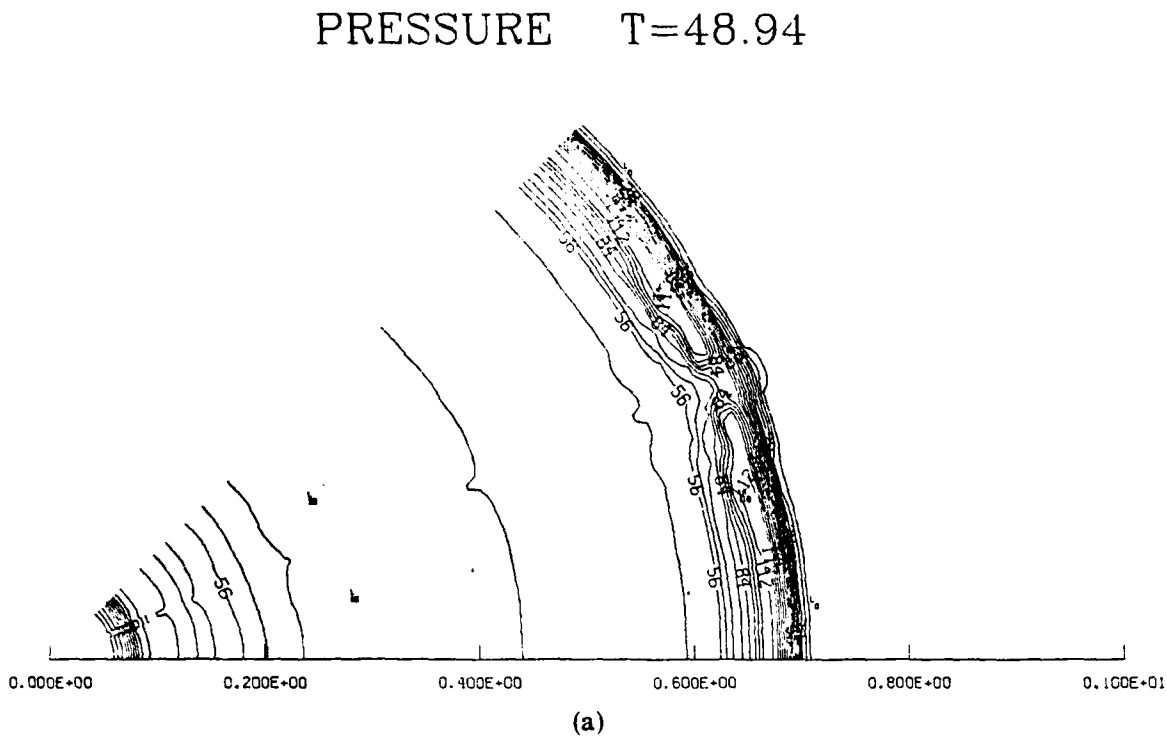

(a)

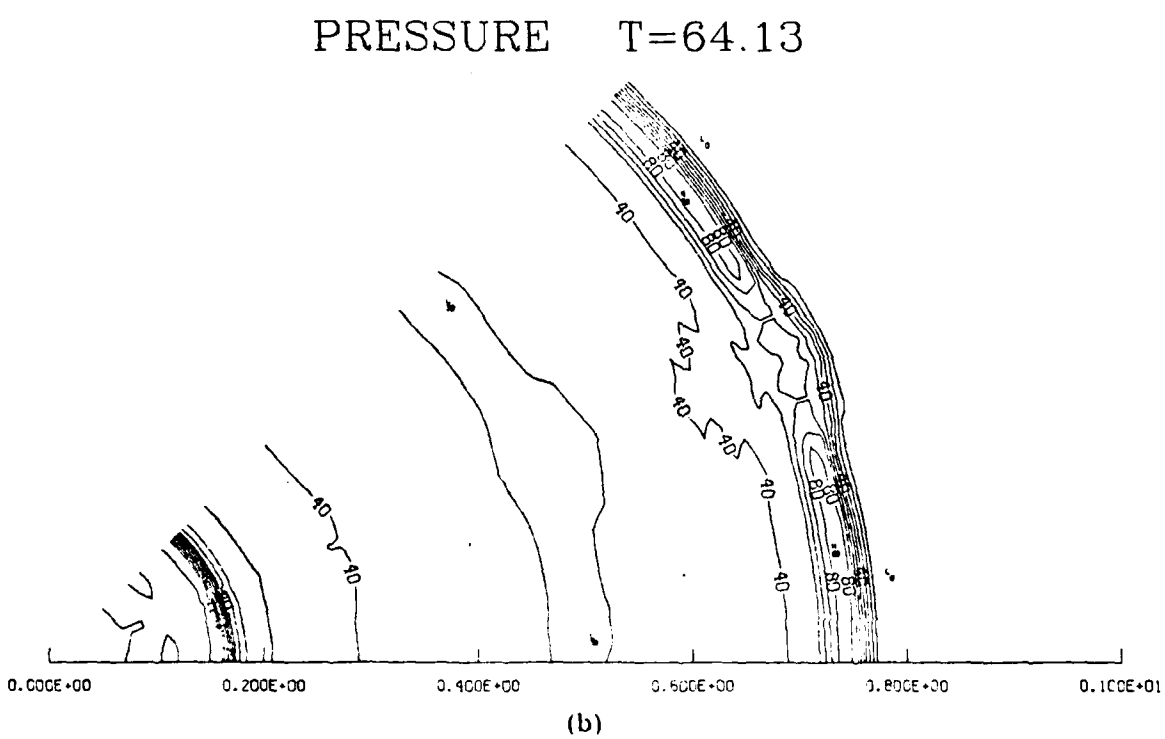

(b)

Fig. 5 — Pressure contours at selected times for a simulation with a constant initial channel temperature. The display format is similar to Figure 1. The contours are labeled in units of 1×10^6 ergs/cm^3. The times displayed are: 5.a = 48.9 ns, 5.b = 64.1 ns, and 5.c = 89.1 ns.

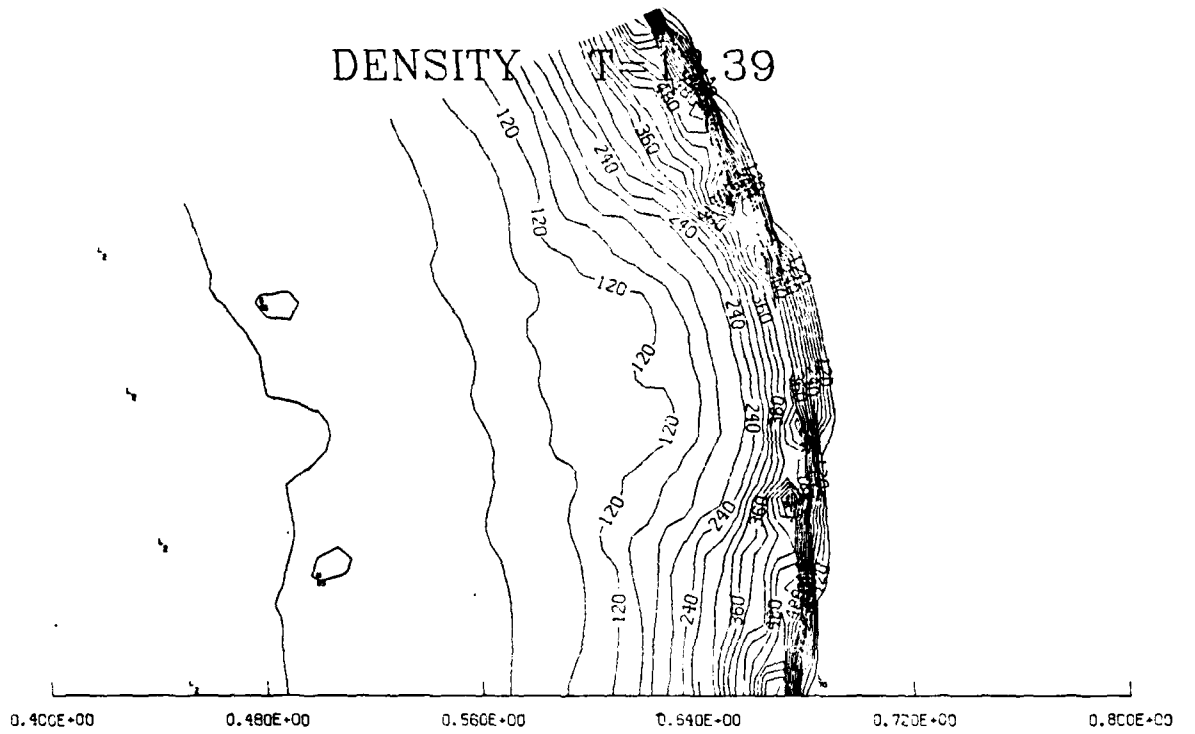

(c)

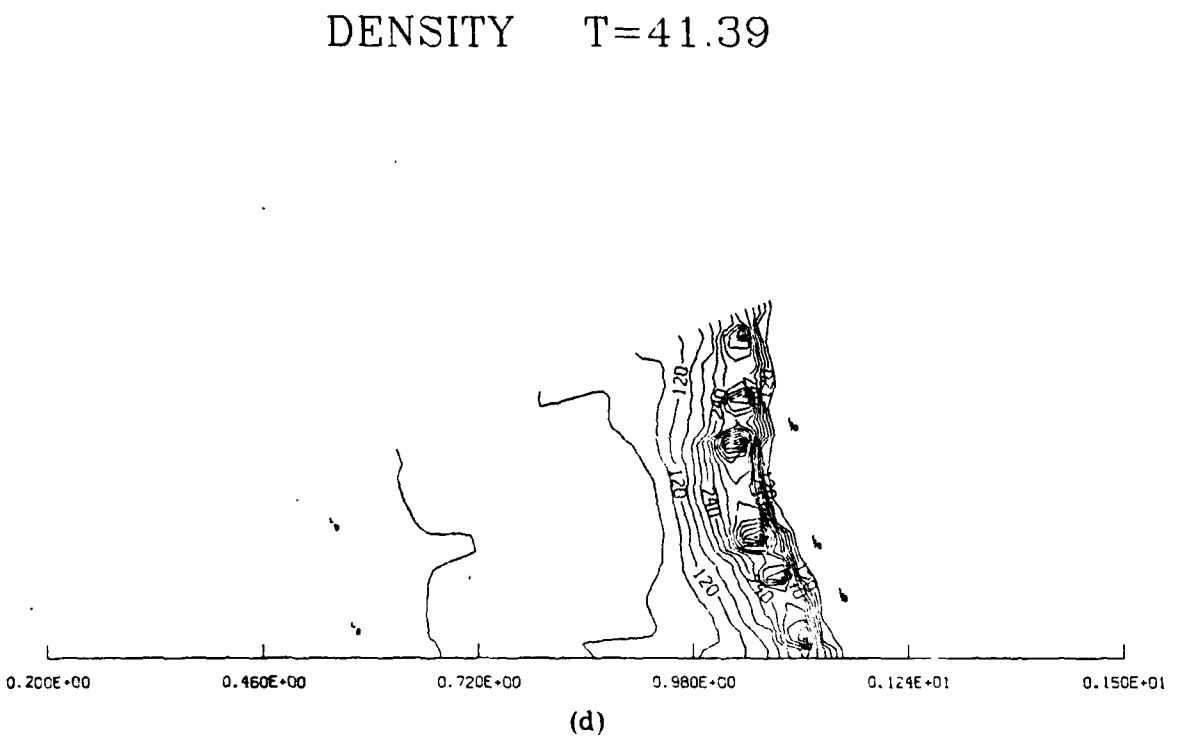

(d)

Fig. 4 (Cont'd) — Density contours at selected times for a "large" jet type of perturbation. Display format is similar to Figure 1. Contours are labeled in units of 10^{-7} gm/cm^3. The times displayed are: 4.a = 2.6 ns, 4.b = 6.09 ns, 4.c = 13.39 ns, and 4.d = 41.4 ns.

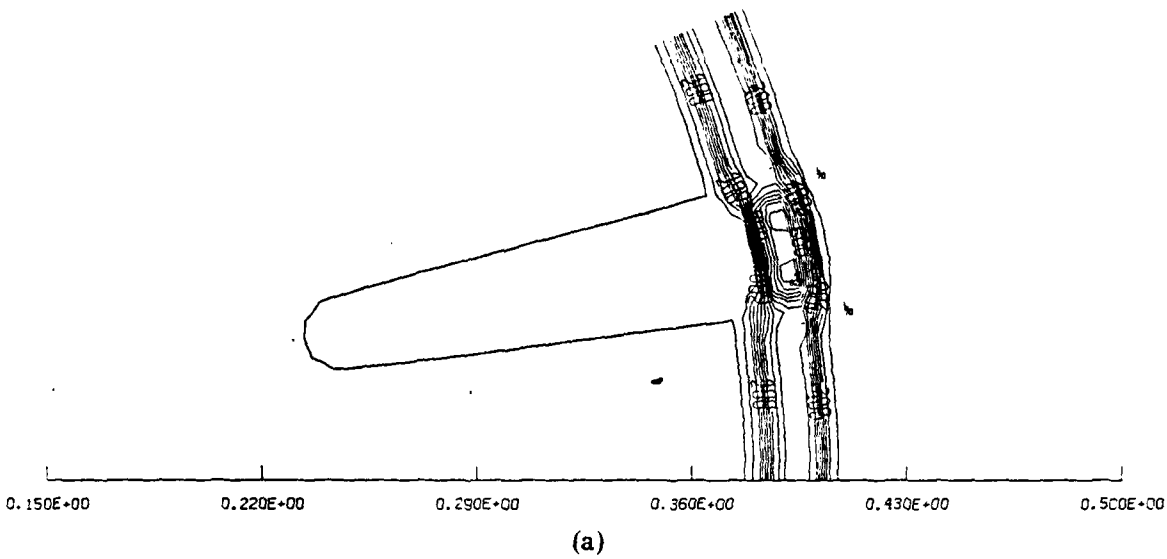

(a)

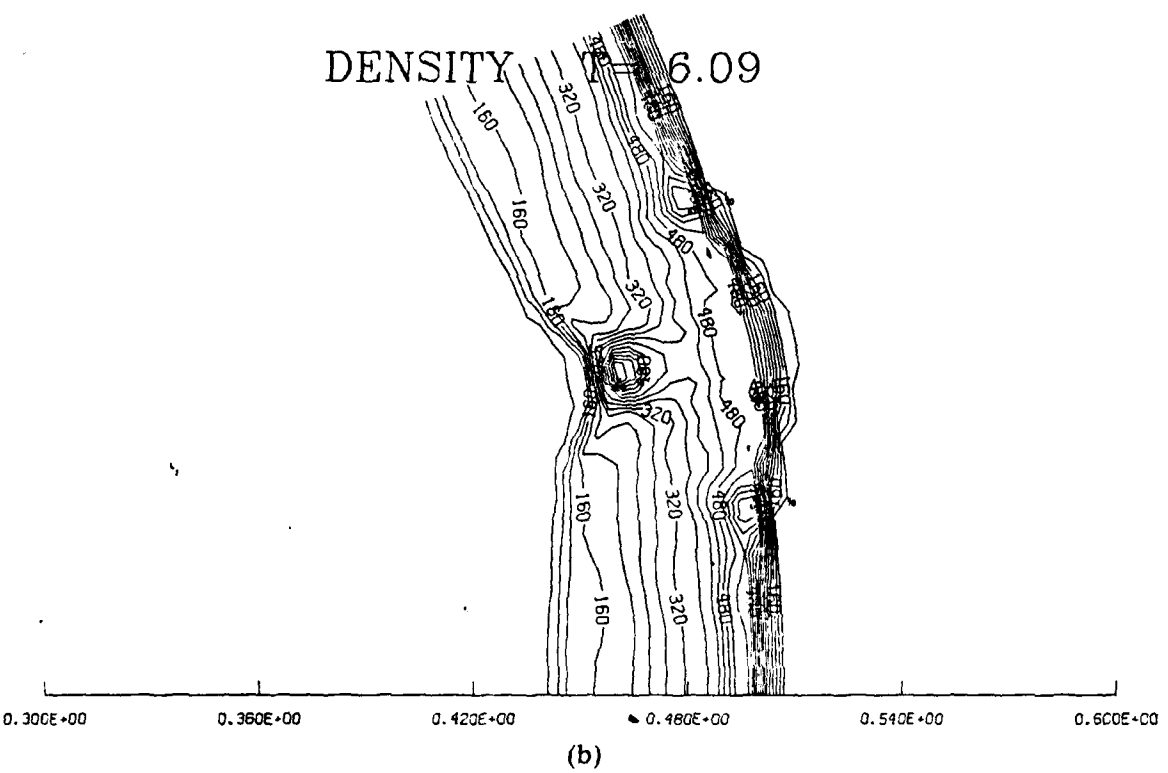

(b)

Fig. 4 — Density contours at selected times for a "large" jet type of perturbation. Display format is similar to Figure 1. Contours are labeled in units of 10^{-7} gm/cm^3. The times displayed are: 4.a = 2.6 ns, 4.b = 6.09 ns, 4.c = 13.39 ns, and 4.d = 41.4 ns.

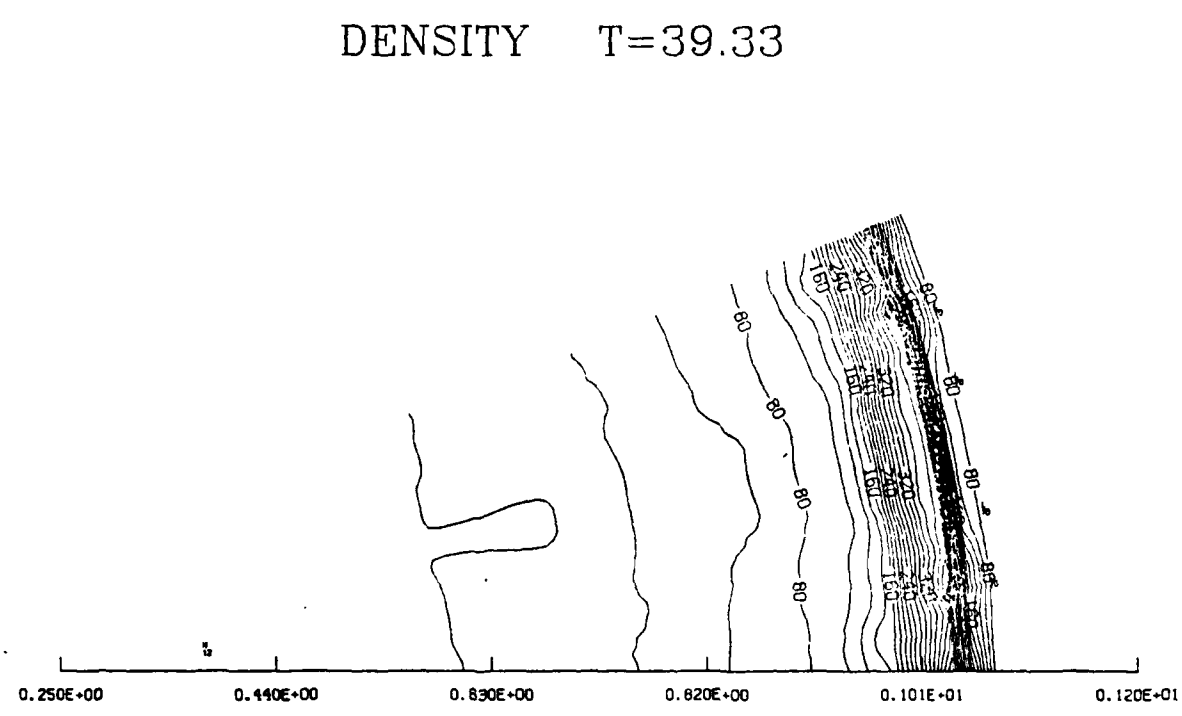

(c)

Fig. 3 (Cont'd) — Density contours at selected times for a "small" jet type of perturbation. Display format is similar to Figure 1. Contours are labeled in units of 10^{-7} gm/cm^3. The times displayed are: 3.a = 2.6 ns, 3.b = 5.89 ns, and 3.c = 39.3 ns.

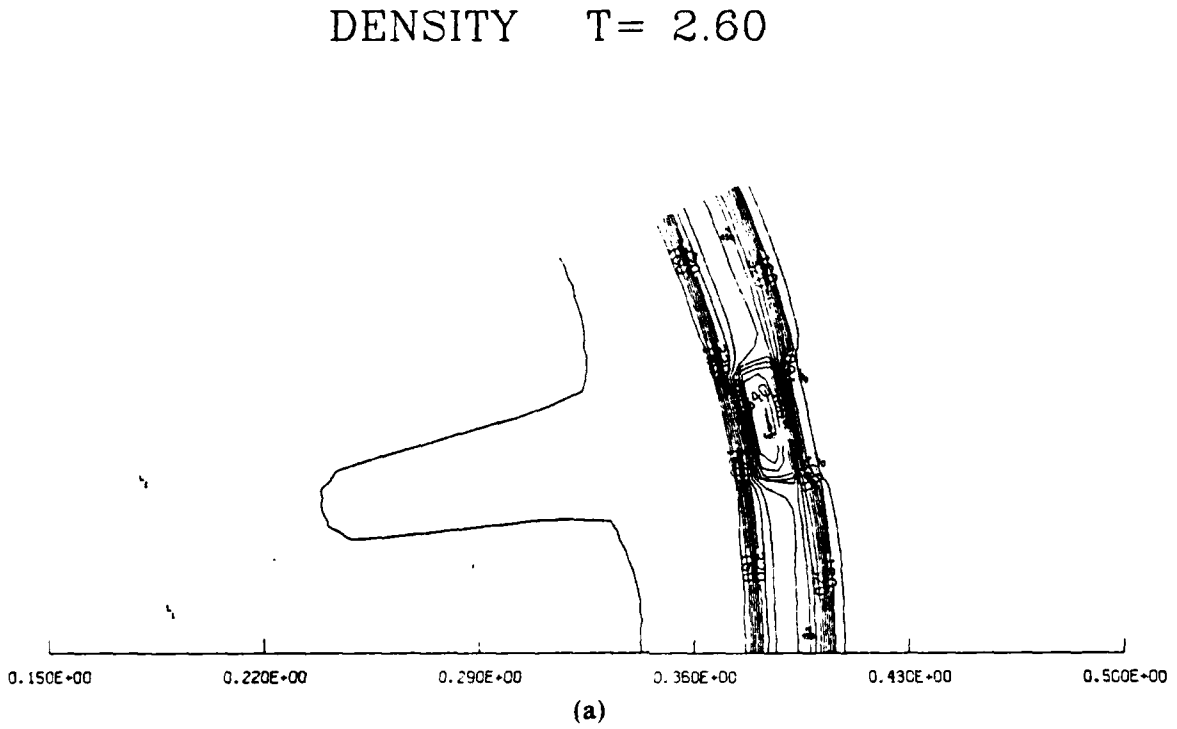

(a)

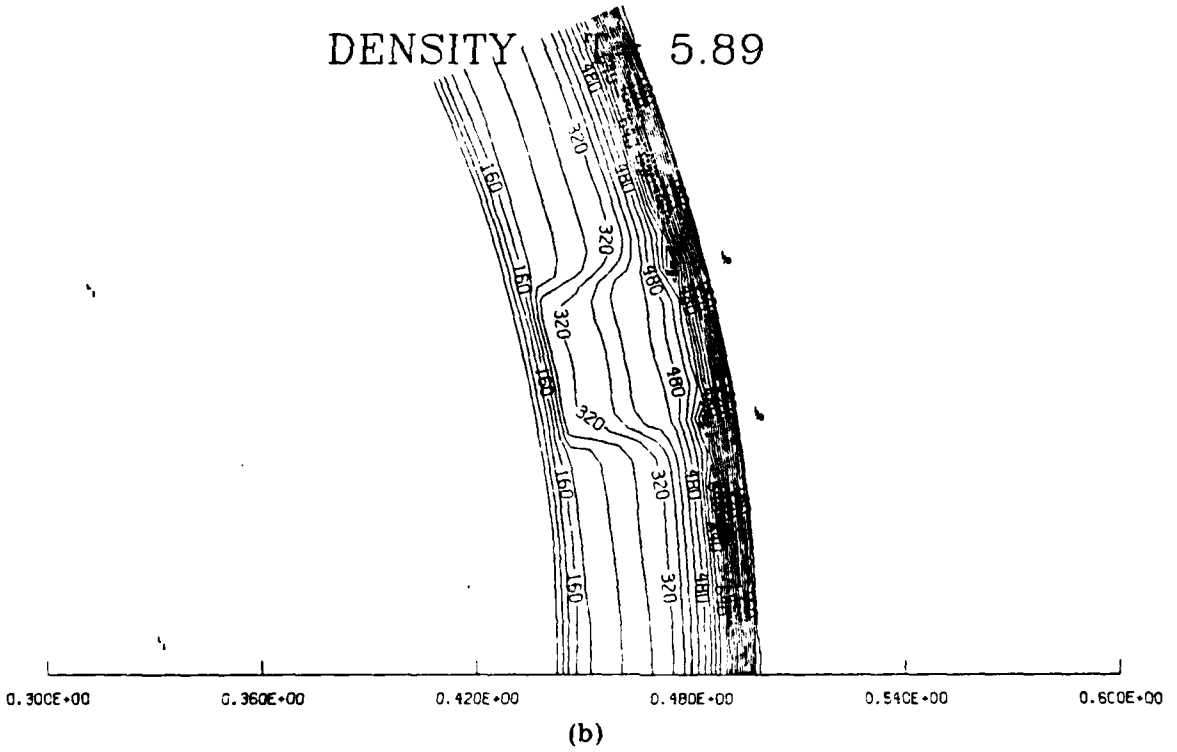

(b)

Fig. 3 — Density contours at selected times for a "small" jet type of perturbation. Display format is similar to Figure 1. Contours are labeled in units of 10^{-7} gm/cm^3. The times displayed are: 3.a = 2.6 ns, 3.b = 5.89 ns, and 3.c = 39.3 ns.

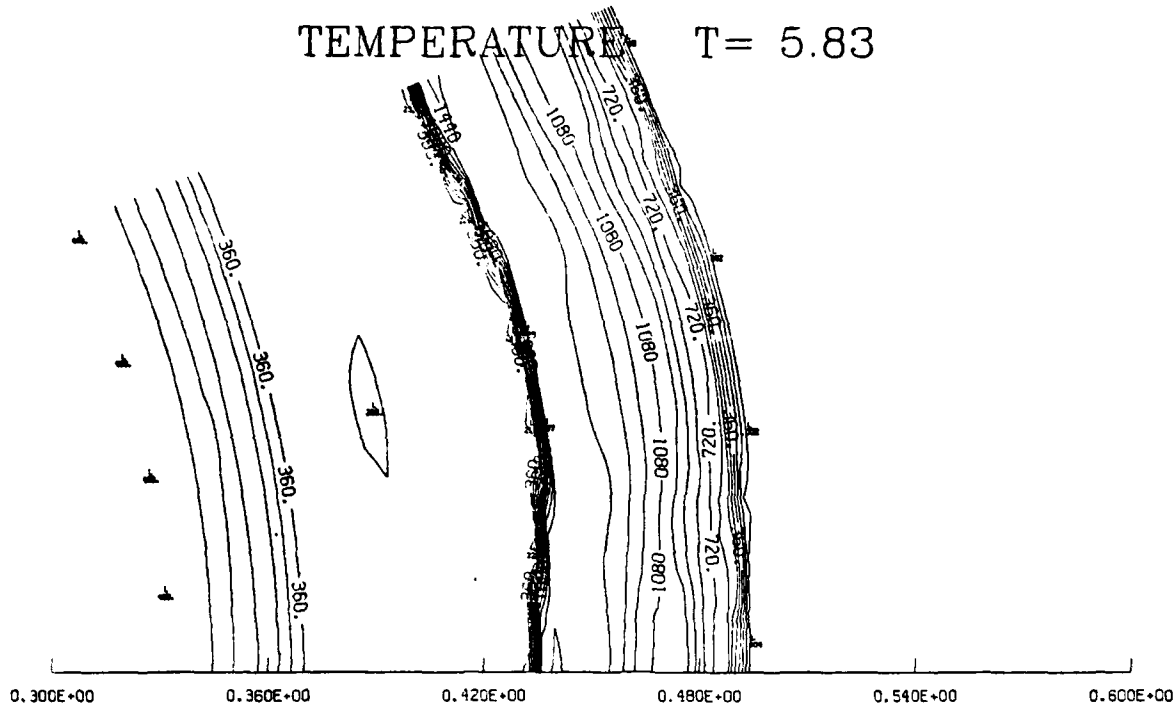

(a)

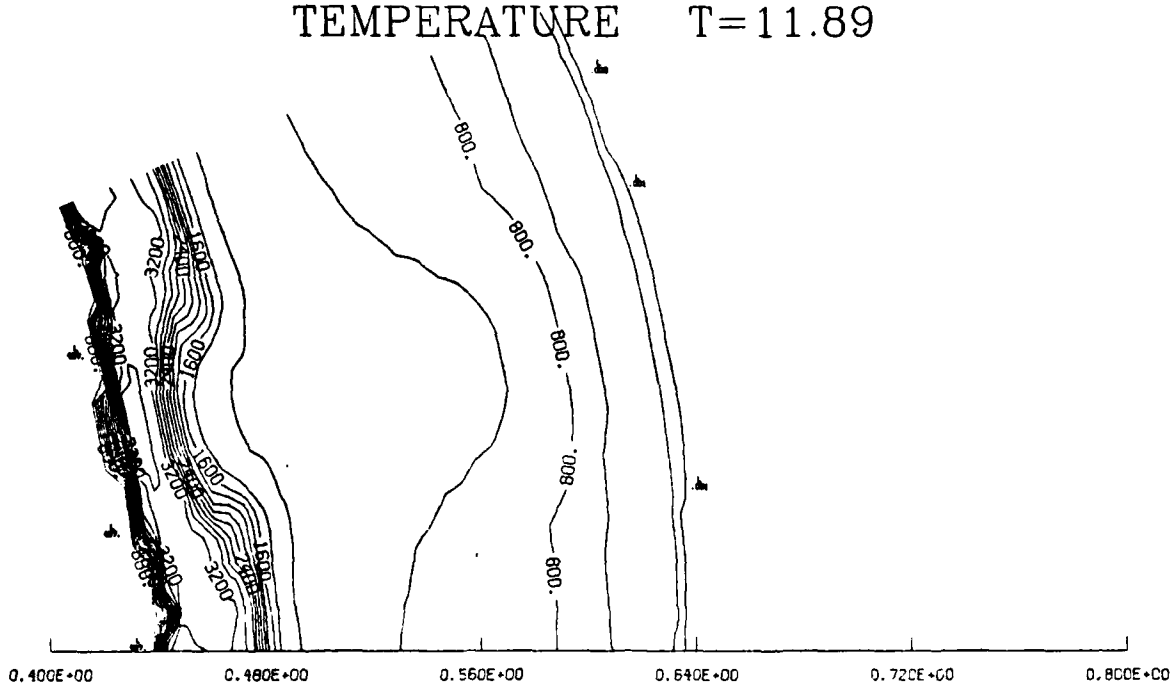

(b)

Fig. 2 — Similar to Figure 1 except the temperature is displayed. The times displayed are: 2.a = 5 83 ns and 2.b = 11.89 ns.

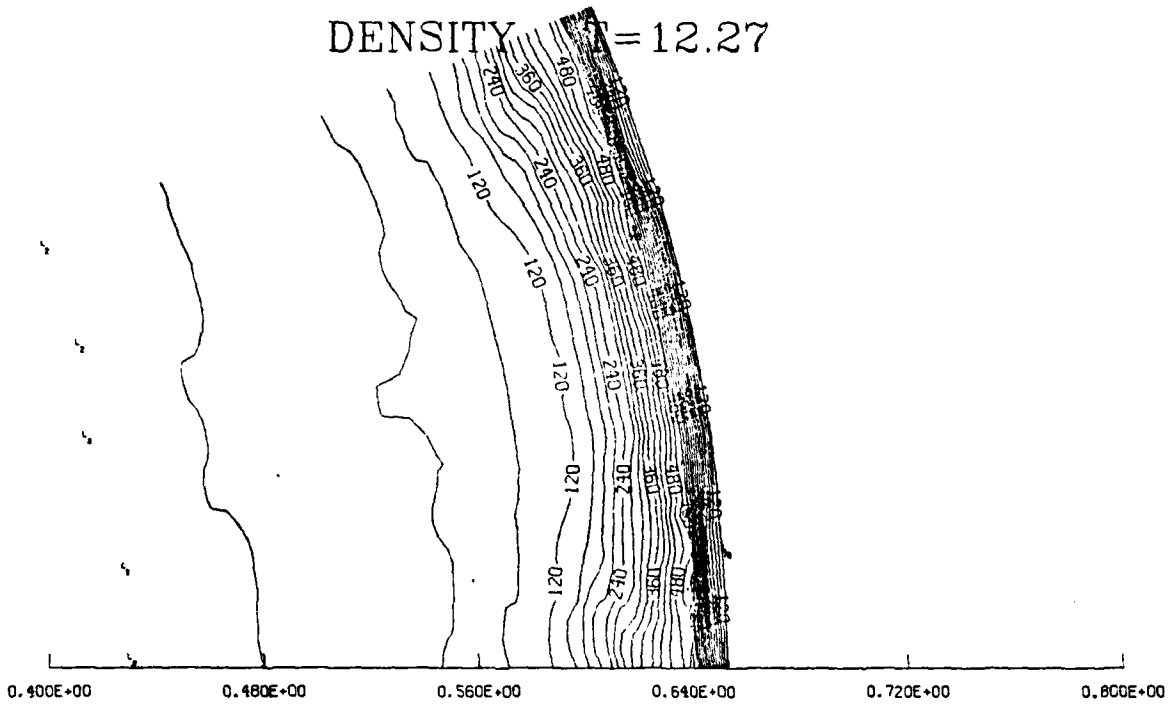

(c)

Fig. 1 (Cont'd) — Density contours at selected times for a debris shell with an initial sinusoidal density perturbation. The data is contoured on an angular wedge shaped area. The bottom axis gives the radial distance along that edge of the wedge. Contours are labeled in units of 10^{-7} gm/cm^3. The times displayed are: 1.a = 2.58 ns, 1.b = 5.86 ns, 1.c = 12.27 ns.

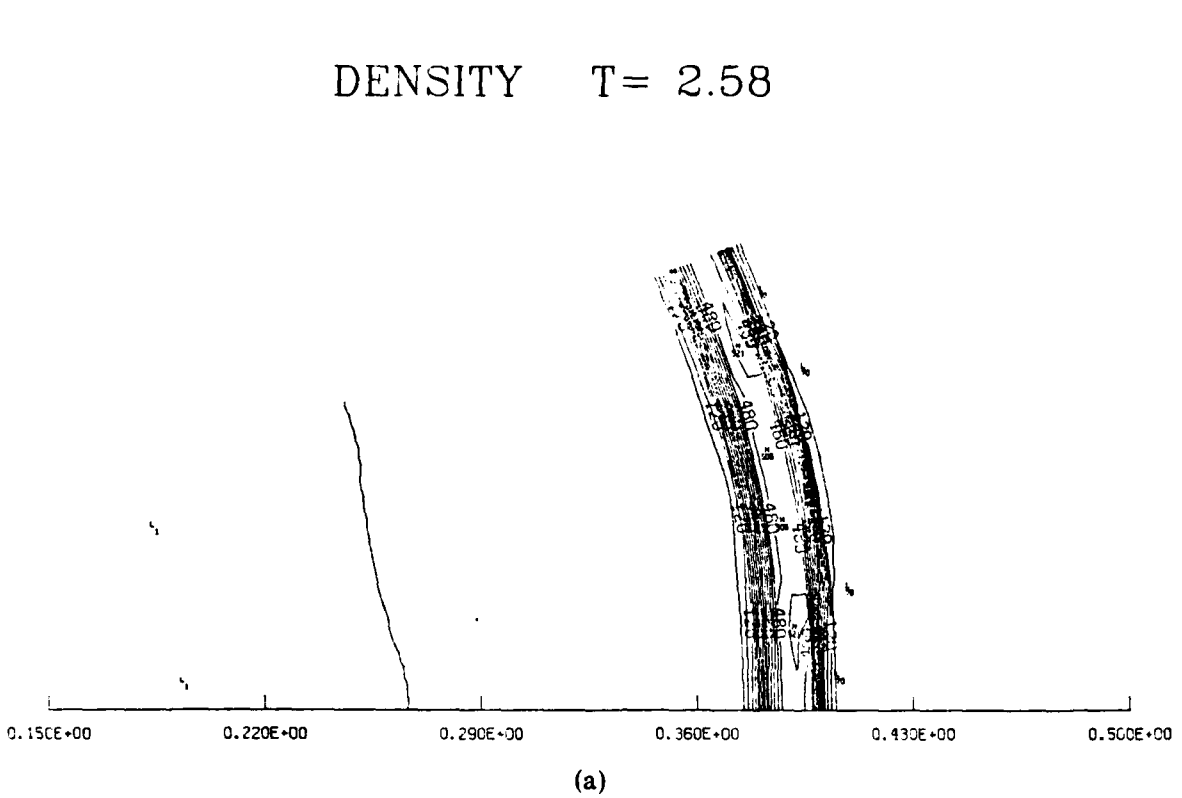

(a)

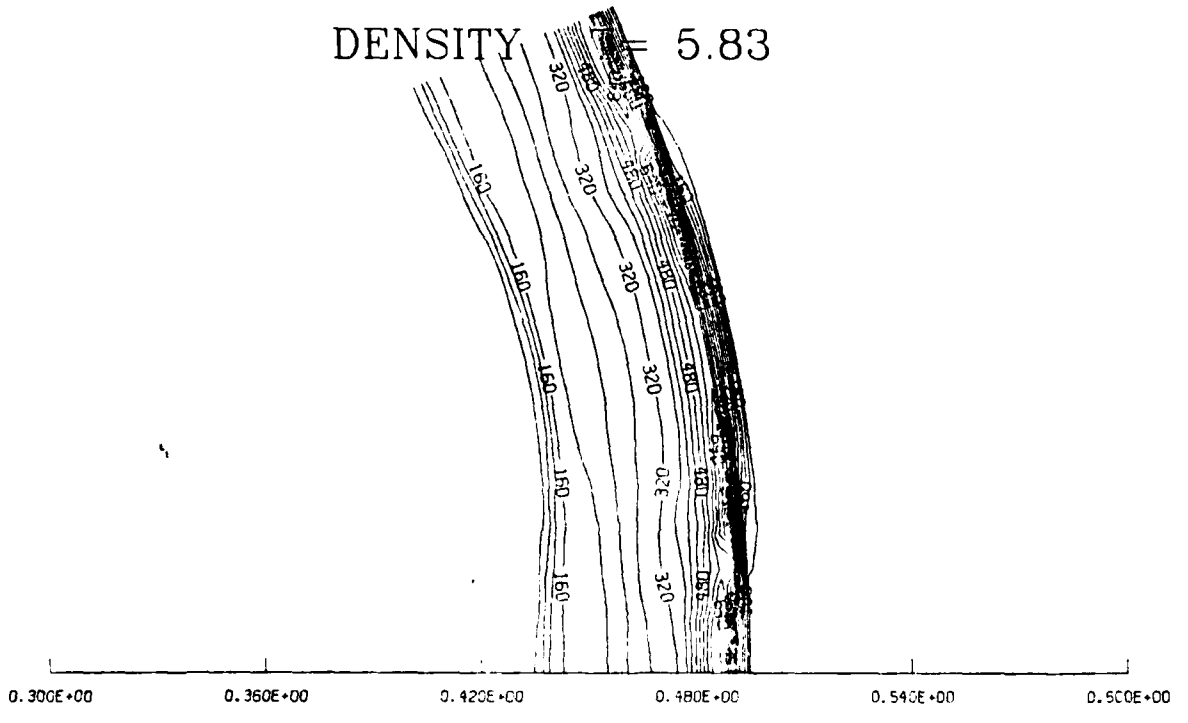

(b)

Fig. 1 — Density contours at selected times for a debris shell with an initial sinusoidal density perturbation. The data is contoured on an angular wedge shaped area. The bottom axis gives the radial distance along that edge of the wedge. Contours are labeled in units of 10^{-7} gm/cm^3. The times displayed are: 1.a = 2.58 ns, 1.b = 5.86 ns, 1.c = 12.27 ns.

Giuliani (1984) has suggested an interesting mechanism for the aneurysms which depends on the thermal conductivity being high in the region of the aneurysm and low elsewhere. The most plausible reason for this is a magnetic field which is present everywhere in the shell except the aneurysm. Keskinen (1983) has pointed out how self-generated magnetic fields can be produced in the initial laser expansion. The same mechanism can also operate within the region that bounds the main shell from the lower density region produced by the channel. The rate at which self-generated magnetic fields are produced is (*e.g.* Tidman, 1975)

$$\frac{\partial \vec{B}}{\partial t} = \frac{cm_i}{\rho^2 e} \nabla P \times \nabla \rho. \tag{10}$$

This requires that the pressure gradient and the density gradient be in somewhat different directions. Reference to Figures 5 and 6 show that in the channel region it is quite possible for the gradients to be misaligned. The misalignment can be as high as 15-20°. Typical gradient scale lengths for the pressure and density are of the order of .05 cm or less at the channel boundary. With $\rho \approx 2 \times 10^{-5}$ gm/cm^3 and $P \approx 10^8$ erg/cm^3, we get $\partial \vec{B}/\partial t \sim 10^{12}$ G/sec for a 10° misalignment. Taken at face value, this result would imply that kiloGauss fields could be generated at the channel boundary. This is quite likely a gross over-estimate. However, it does indicate that self-generated magnetic fields may be quite important for the evolution of the pre-heated channels. In particular, it gives a natural way in which Giuliani's mechanism can be seeded and maintained, since the self-generated magnetic field at the channel boundary will suppress thermal conduction from the channel region to the rest of the shell.

Acknowledgments

This work was supported by the Defense Nuclear Agency.

ambient medium. The temperature at the center of the channel was given by

$$T_{ch} = 200 \text{ eV} \left(\frac{r}{0.3 \text{ cm}}\right)^2 \exp(-(r - 0.3 \text{ cm})/0.3 \text{ cm})$$

This gives a very high energy of 200 eV at the edge of the debris region initially. The energy drops very rapidly, however, to less than 2 eV at 1 cm from the target. The intent here was to see if a channel could be opened at very early times in the calculation, and once opened whether the bulge created could be maintained or grow as the shock ran into less evacuated regions. Figure 7 shows the pressure profiles at 49, 67, and 95 ns into the calculation. Figure 7.a (49 ns) shows a bulge that is consistent with the size of aneurysms seen at that stage of the blast wave expansion. On the other hand, the succeeding two figures show the bulge damping while simulataneously broadening. It is clear that once the perturbation in ambient density into which the blast wave runs dies out, so does the bulge in the shock front.

IV. Discussion

Two-dimensional gas-dynamic simulations of the NRL laser experiment have been performed to study the formation of aneurysms in the blast wave, and to study the formation of structure internal to the blast wave itself. Two sets of simulations have been performed: perturbed debris shell and pre-heated channel.

The conclusions from the perturbed debris shell simulations are summarized as follows. The source of the aneurysms observed in the NRL laser experiment is probably not due to perturbations of the debris shell. No "simple" perturbation of the shell leads to the appearance of a simple bump growing on the surface of the blast wave. The heuristic arguments about the stability of blast waves seem to be vindicated by this set of simulations. On the other hand, a large amount of structure can be produced relatively easily internal to the shock front. With suitable perturbations it appears that density enhancements of a factor of two may be possible. Further work is needed, however, to determine how general such large density jumps may be.

On the other hand, the simulations using a pre-heated channel show that such a channel can effectively produce a distortion in the spherical shape of an expanding blast wave. However, it appears that the magnitude of the distortion is too small to explain the aneurysms. Another problem with the pre-heated channel explanation is that the aneurysms seem to have the highest density of any region of the shock front. The simulations show the bulges having somewhat lower density than the surrounding shock. It is unlikely that a pre-heated channel can be the full explanation of the aneurysms.

B. Results

In the first simulation the channel was assumed to have a constant angular width and the same pressure everywhere along the central axis initially. The pressure corresponded to a thermal energy of 4 eV per particle. This is perhaps the largest energy that could be deposited in a channel without producing much higher values than are seen by the spectroscopic diagnostics which sample a long line of sight through which the channel might run. This particular type of initial condition favors the development of the aneurysm at late times in the calculation. This is born out by Figure 5, which shows the time development of the pressure in this calculation. We plot the pressure because it gives a better indication of the shock strength than does the density. In Figures 5.a – 5.c at times 49, 64, and 89 ns into the calculation, respectively, we can see a slight protuberance of the shock front developing and increasing in both in distance ahead of the rest of the shock, and, most particularly, in its angular extent. Figure 6, which plots the density at 64 and 89 ns, shows the same effect. Also apparent is the decrease in density in the channel. In Figure 6.b the minimum density in the channel just ahead of the shock is almost a factor of 2 below the ambient. Even at the earlier time, the density decrease is about 40%. It is clear that the position of the shock front in the channel does not show the increase in speed that would be expected if were following its own blast wave shock radius-time relation. Interestingly enough, however, if we solve the blast wave relation for the ratio of P/ρ as a function of time, we find that it goes as

$$\frac{P}{\rho} \propto v_{sh}^2 \propto \left(\frac{E_{bl}}{\rho_0}\right)^{0.4} t^{-1.2}. \tag{9}$$

The jump in the density ratio from channel to ambient is 2. The pressure ratio jump just behind the shock is about 5/7. This is quite close to the value that would be predicted by (9) by changing the density by a factor of two. In this particular respect, then, the shock propagation within the channel does follow the blast wave relation. The reason that the shock within the channel does not run way ahead of the the rest of the channel is that the bulge has a significantly larger surface area than the area on a sphere with the unperturbed blast wave radius which subtends the same solid angle from the center of the explosion. The energy of the shock is thus spread over a larger area, and the shock speed slows down over what it would be in a strictly spherical expansion. The fact that the pressure jump is about right for a blast wave solution suggests that the volume into which the set amount of energy flows is about the same as it would be for a purely spherical expansion.

The second simulation in this sequence used a different initialization of the channel to attempt to mimic a diverging beam which was also absorbed by the

Energy

$$\frac{\partial E}{\partial t} = -\frac{1}{r^2}\frac{\partial}{\partial r} r^2 v_r (E+P) - \frac{1}{r\sin\theta}\frac{\partial}{\partial \theta}\sin\theta\, v_\theta (E+P) \qquad (8.d)$$

where

$$E \equiv \frac{1}{2}\rho({v_\theta}^2 + {v_r}^2) + \frac{P}{\gamma - 1}$$
$$p_\theta \equiv \rho v_\theta$$
$$p_r \equiv \rho v_r$$
$$\gamma \equiv \text{ratio of specific heats}$$

and the polar angle, θ, is taken to be the angle from the axis of the channel. The same rezoning technique used in § II was used again here to increase resolution in the region of the shock front.

We will discuss two simulations below, both of which assume a laser energy of 10 J and an ambient pressure of 5 Torr. The initial conditions used have for R <0.3 cm from the target

$$\rho = \rho_a + \rho_d = 9 \times 10^{-6} \text{ gm/cm}^3$$
$$v_r = \frac{\rho_d}{\rho_a + \rho_d} v_d = 128 \text{ km/sec}$$
$$P = \frac{(\gamma - 1)\rho_d v_d^2}{2}\left(1 - \frac{\rho_d}{\rho_a + \rho_d}\right) = 5 \times 10^8 \text{ erg/cm}^3$$

where the a and d subscripts refer to ambient and debris, respectively. The debris velocity was assumed to be the 575 km/sec used in the previous section and the debris mass was scaled down by the ratio of 10/38, giving a debris density $\approx 2 \times 10^{-6}$ gm/cm^3. It is assumed that ambient and debris material are mixed uniformly and have fully coupled. For $R > 0.3$ cm from the target, the ambient gas is assumed to have a temperature of 0.5 eV except in the channel. The energy deposited in the channel is assumed to have a Gaussian θ dependence – $E_{ch} \propto \exp(-\theta^2/2\theta_c^2)$ – and in both simulations $\theta_c = 0.07$ radians. In the first simulation a constant channel energy of 4 eV was assumed, while in the second the form used atttempted to mimic a spreading beam with absorption by the ambient gas.

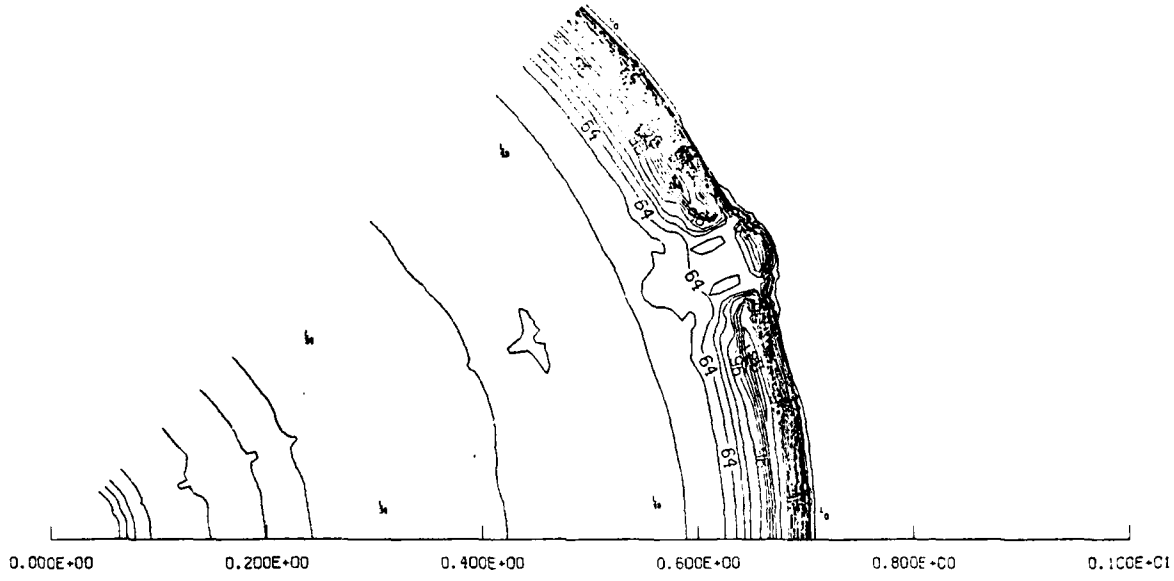

(a)

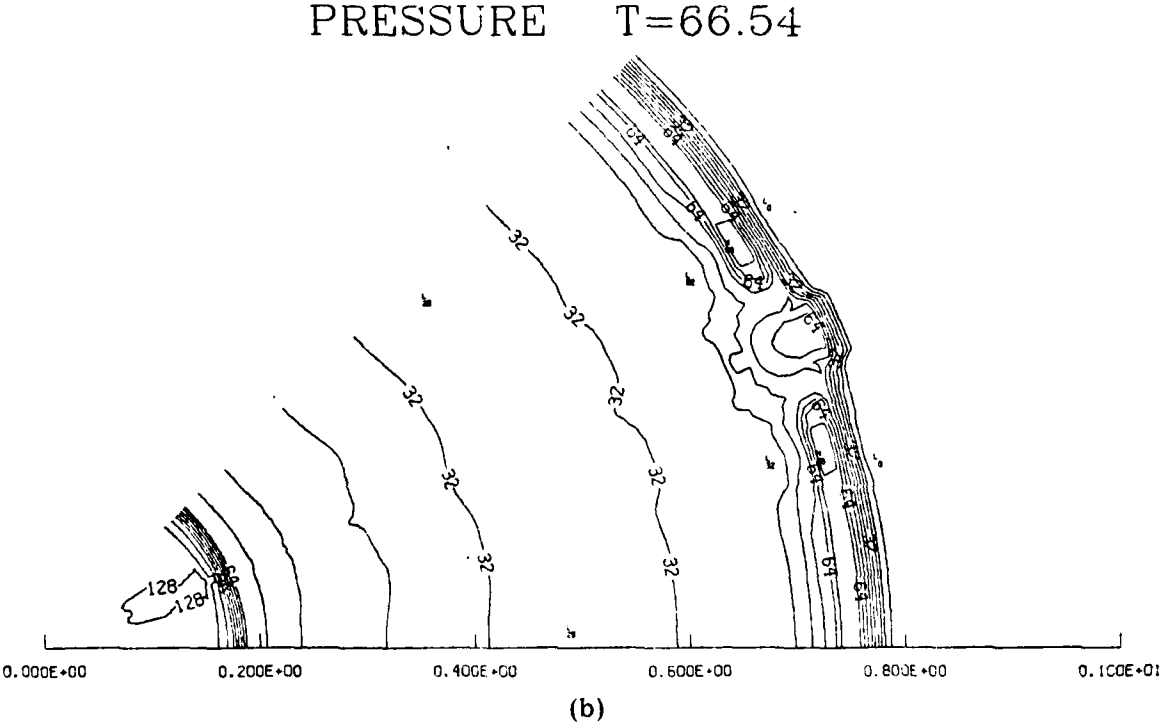

(b)

Fig. 7 — Pressure contours at selected times for a simulation with an initialization to mimic a diverging beam with ambient absorption. The display format is similar to Figure 1. The contours are labeled in units of 1×10^6 ergs/cm^3. The times displayed are 7.a = 49.4 ns 7.b = 66.5 ns, and 7.c = 94.6 ns.

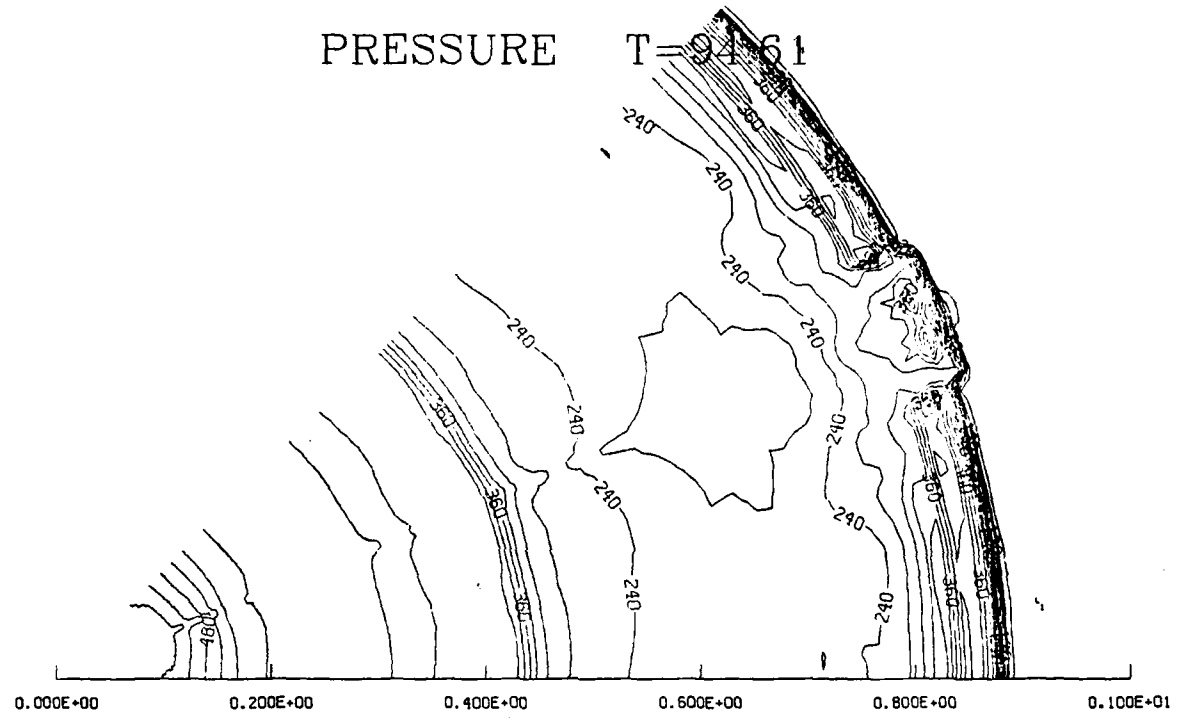

(c)

Fig. 7 (Cont'd) — Pressure contours at selected times for a simulation with an initialization to mimic a diverging beam with ambient absorption. The display format is similar to Figure 1. The contours are labeled in units of 1×10^6 ergs/cm^3. The times displayed are 7.a = 49.4 ns, 7.b = 66.5 ns, and 7.c = 94.6 ns.

References

V.A. Andronov, S.M. Bakhrakh, E.E. Meshkov, V.N. Mokhov, V.V. Nikiforov, A.V. Pevnitskii, and A.I. Toishmyakov, "Turbulent mixing at contact surface accelerated by shock waves", *Sov. Phys. JETP*, **44**, 424, 1976.

J.L. Giuliani, "Thermal evaporation in blast waves: a model for aneurism formation in the NRL laser-HANE simulation experiment", *NRL Memorandum Report* 5420, October 11, 1984. (AD-A147 006)

K. Hain, "The partial donor cell method", *NRL Memorandum Report 3713*, 1978. (AD-A053 387)

M.J. Keskinen, "Analytic models of magnetic field evolution in laser-produced plasma expansions", *NRL Memorandum Report 5163*, 1983. (AD-A132 181)

J.G. Lyon, "The partial donor cell method: extensions and generalizations", in preparation, 1984.

R.D. Richtmeyer, "Taylor instability in shock acceleration of compressible fluids", *Communications on Pure and Applied Math.*, **13**, 297-319, 1960.

B.H. Ripin, private communication, 1983.

J.A. Stamper, B.H. Ripin, E.A. Mclean, and S.P. Obenschain, "Optical imaging of a coupling region between inter-streaming plasmas", *NRL Memorandum Report 5278*, 1984. (AD-A139 191)

D.A. Tidman, "Thermally generated magnetic fields in laser-driven compressions and explosions", *Phys. of Fluids*, **18**, 1454-1459, 1975.

G.B. Whitham, *Linear and Nonlinear Waves*, John Wiley and Sons, New York, 1974.

DISTRIBUTION LIST

DEPARTMENT OF DEFENSE

ASSISTANT SECRETARY OF DEFENSE
COMM, CMD, CONT 7 INTELL
WASHINGTON, D.C. 20301

DIRECTOR
COMMAND CONTROL TECHNICAL CENTER
PENTAGON RM BE 685
WASHINGTON, D.C. 20301
01CY ATTN C-650
01CY ATTN C-312 R. MASON

DIRECTOR
DEFENSE ADVANCED RSCH PROJ AGENCY
ARCHITECT BUILDING
1400 WILSON BLVD.
ARLINGTON, VA. 22209
01CY ATTN NUCLEAR
MONITORING RESEARCH
01CY ATTN STRATEGIC TECH OFFICE

DEFENSE COMMUNICATION ENGINEER CENTER
1860 WIEHLE AVENUE
RESTON, VA. 22090
01CY ATTN CODE R410
01CY ATTN CODE R812

DEFENSE TECHNICAL INFORMATION CENTER
CAMERON STATION
ALEXANDRIA, VA. 22314
02CY

DIRECTOR
DEFENSE NUCLEAR AGENCY
WASHINGTON, D.C. 20305
01CY ATTN STVL
04CY ATTN TITL
01CY ATTN DDST
03CY ATTN RAAE

COMMANDER
FIELD COMMAND
DEFENSE NUCLEAR AGENCY
KIRTLAND, AFB, NM 87115
01CY ATTN FCPR

DEFENSE NUCLEAR AGENCY
SAO/DNA
BUILDING 20676
KIRTLAND AFB, NM 87115
01CY D.C. THORNBURG

DIRECTOR
INTERSERVICE NUCLEAR WEAPONS SCHOOL
KIRTLAND AFB, NM 87115
01CY ATTN DOCUMENT CONTROL

JOINT CHIEFS OF STAFF
WASHINGTON, D.C. 20301
01CY ATTN J-3 WWMCCS EVALUATION
OFFICE

DIRECTOR
JOINT STRAT TGT PLANNING STAFF
OFFUTT AFB
OMAHA, NB 68113
01CY ATTN JSTPS/JLKS
01CY ATTN JPST G. GOETZ

CHIEF
LIVERMORE DIVISION FLD COMMAND DNA
DEPARTMENT OF DEFENSE
LAWRENCE LIVERMORE LABORATORY
P.O. BOX 808
LIVERMORE, CA 94550
01CY ATTN FCPRL

COMMANDANT
NATO SCHOOL (SHAPE)
APO NEW YORK 09172
01CY ATTN U.S. DOCUMENTS OFFICER

UNDER SECY OF DEF FOR RSCH & ENGRG
DEPARTMENT OF DEFENSE
WASHINGTON, D.C. 20301
01CY ATTN STRATEGIC & SPACE
SYSTEMS (OS)

WWMCCS SYSTEM ENGINEERING ORG
WASHINGTON, D.C. 20305
01CY ATTN R. CRAWFORD

COMMANDER/DIRECTOR
ATMOSPHERIC SCIENCES LABORATORY
U.S. ARMY ELECTRONICS COMMAND
WHITE SANDS MISSILE RANGE, NM 88002
01CY ATTN DELAS-EO, F. NILES

DIRECTOR
BMD ADVANCED TECH CTR
HUNTSVILLE OFFICE
P.O. BOX 1500
HUNTSVILLE, AL 35807
01CY ATTN ATC-T MELVIN T. CAPPS
01CY ATTN ATC-O W. DAVIES
01CY ATTN ATC-R DON RUSS

PROGRAM MANAGER
BMD PROGRAM OFFICE
5001 EISENHOWER AVENUE
ALEXANDRIA, VA 22333
01CY ATTN DACS-BMT J. SHEA

CHIEF C-E- SERVICES DIVISION
U.S. ARMY COMMUNICATIONS CMD
PENTAGON RM 18269
WASHINGTON, D.C. 20310
01CY ATTN C- E-SERVICES DIVISION

COMMANDER
FRADCOM TECHNICAL SUPPORT ACTIVITY
DEPARTMENT OF THE ARMY
FORT MONMOUTH, N.J. 07703
01CY ATTN DRSEL-NL-RD H. BENNET
01CY ATTN DRSEL-PL-ENV H. BOMKE
01CY ATTN J.E. QUIGLEY

COMMANDER
U.S. ARMY COMM-ELEC ENGRG INSTAL AGY
FT. HUACHUCA, AZ 85613
01CY ATTN CCC-EMEO GEORGE LANE

COMMANDER
U.S. ARMY FOREIGN SCIENCE & TECH CTR
220 7TH STREET, NE
CHARLOTTESVILLE, VA 22901
01CY ATTN DRXST-SD

COMMANDER
U.S. ARMY MATERIAL DEV & READINESS CMD
5001 EISENHOWER AVENUE
ALEXANDRIA, VA 22333
01CY ATTN DRCLDC J.A. BENDER

COMMANDER
U.S. ARMY NUCLEAR AND CHEMICAL AGENCY
7500 BACKLICK ROAD
BLDG 2073
SPRINGFIELD, VA 22150
01CY ATTN LIBRARY

DIRECTOR
U.S. ARMY BALLISTIC RESEARCH
LABORATORY
ABERDEEN PROVING GROUND, MD 21005
01CY ATTN TECH LIBRARY,
EDWARD BAICY

COMMANDER
U.S. ARMY SATCOM AGENCY
FT. MONMOUTH, NJ 07703
01CY ATTN DOCUMENT CONTROL

COMMANDER
U.S. ARMY MISSILE INTELLIGENCE AGENCY
REDSTONE ARSENAL, AL 35809
01CY ATTN JIM GAMBLE

DIRECTOR
U.S. ARMY TRADOC SYSTEMS ANALYSIS
ACTIVITY
WHITE SANDS MISSILE RANGE, NM 88002
01CY ATTN ATAA-SA
01CY ATTN TCC/F. PAYAN JR.
01CY ATTN ATTA-TAC LTC J. HESSE

COMMANDER
NAVAL ELECTRONIC SYSTEMS COMMAND
WASHINGTON, D.C. 20360
01CY ATTN NAVALEX 034 T. HUGHES
01CY ATTN PME 117
01CY ATTN PME 117-T
01CY ATTN CODE 5011

COMMANDING OFFICER
NAVAL INTELLIGENCE SUPPORT CTR
4301 SUITLAND ROAD, BLDG. 5
WASHINGTON, D.C. 20390
01CY ATTN MR. DUBBIN STIC 12
01CY ATTN NISC-50
01CY ATTN CODE 5404 J. GALET

COMMANDER
NAVAL OCCEAN SYSTEMS CENTER
SAN DIEGO, CA 92152
01CY ATTN J. FERGUSON

NAVAL RESEARCH LABORATORY
WASHINGTON, D.C. 20375
01CY ATTN CODE 4700 S. L. Ossakow
26 CYS IF UNCLASS. 1 CY
IF CLASS)
01CY ATTN CODE 4701 I Vitkovitsky
01CY ATTN CODE 4780 J. Huba (50
CYS IF UNCLASS, 1 CY IF CLASS)
01CY ATTN CODE 7500
01CY ATTN CODE 7550
01CY ATTN CODE 7580
01CY ATTN CODE 7551
01CY ATTN CODE 7555
01CY ATTN CODE 4730 E. MCLEAN
01CY ATTN CODE 4108
01CY ATTN CODE 4730 B. RIPIN
20CY ATTN CODE 2628

COMMANDER
NAVAL SPACE SURVEILLANCE SYSTEM
DAHLGREN, VA 22448
01CY ATTN CAPT J.H. BURTON

OFFICER-IN-CHARGE
NAVAL SURFACE WEAPONS CENTER
WHITE OAK, SILVER SPRING, MD 20910
01CY ATTN CODE F31

DIRECTOR
STRATEGIC SYSTEMS PROJECT OFFICE
DEPARTMENT OF THE NAVY
WASHINGTON, D.C. 20376
01CY ATTN NSP-2141
01CY ATTN NSSP-2722 FRED WIMBERLY

COMMANDER
NAVAL SURFACE WEAPONS CENTER
DAHLGREN LABORATORY
DAHLGREN, VA 22448
01CY ATTN CODE DF-14 R. BUTLER

OFFICER OF NAVAL RESEARCH
ARLINGTON, VA 22217
01CY ATTN CODE 465
01CY ATTN CODE 461
01CY ATTN CODE 402
01CY ATTN CODE 420
01CY ATTN CODE 421

COMMANDER
AEROSPACE DEFENSE COMMAND/DC
DEPARTMENT OF THE AIR FORCE
ENT AFB, CO 80912
01CY ATTN DC MR. LONG

COMMANDER
AEROSPACE DEFENSE COMMAND/XPD
DEPARTMENT OF THE AIR FORCE
ENT AFB, CO 80912
01CY ATTN XPDQQ
01CY ATTN XP

AIR FORCE GEOPHYSICS LABORATORY
HANSCOM AFB, MA 01731
01CY ATTN OPR HAROLD GARDNER
01CY ATTN LKB
KENNETH S.W. CHAMPION
01CY ATTN OPR ALVA T. STAIR
01CY ATTN PHD JURGEN BUCHAU
01CY ATTN PHD JOHN P. MULLEN

AF WEAPONS LABORATORY
KIRTLAND AFT, NM 87117
01CY ATTN SUL
01CY ATTN CA ARTHUR H. GUENTHER
01CY ATTN NTYCE 1LT. G. KRAJEI

AFTAC
PATRICK AFB, FL 32925
01CY ATTN TN

AIR FORCE AVIONICS LABORATORY
WRIGHT-PATTERSON AFB, OH 45433
01CY ATTN AAD WADE HUNT
01CY ATTN AAD ALLEN JOHNSON

DEPUTY CHIEF OF STAFF
RESEARCH, DEVELOPMENT, & ACQ
DEPARTMENT OF THE AIR FORCE
WASHINGTON, D.C. 20330
01CY ATTN AFRDQ

HEADQUARTERS
ELECTRONIC SYSTEMS DIVISION
DEPARTMENT OF THE AIR FORCE
HANSCOM AFB, MA 01731
01CY ATTN J. DEAS

HEADQUARTERS
ELECTRONIC SYSTEMS DIVISION/YSEA
DEPARTMENT OF THE AIR FORCE
HANSCOM AFB, MA 01732
01CY ATTN YSEA

HEADQUARTERS
ELECTRONIC SYSTEMS DIVISION/DC
DEPARTMENT OF THE AIR FORCE
HANSCOM AFB, MA 01731
01CY ATTN DCKC MAJ J.C. CLARK

COMMANDER
FOREIGN TECHNOLOGY DIVISION, AFSC
WRIGHT-PATTERSON AFB, OH 45433
01CY ATTN NICD LIBRARY
01CY ATTN ETDP B. BALLARD

COMMANDER
ROME AIR DEVELOPMENT CENTER, AFSC
GRIFFISS AFB, NY 13441
01CY ATTN DOC LIBRARY/TSLD
01CY ATTN OCSE V. COYNE

SAMSO/SZ
POST OFFICE BOX 92960
WORLDWAY POSTAL CENTER
LOS ANGELES, CA 90009
(SPACE DEFENSE SYSTEMS)
01CY ATTN SZJ

STRATEGIC AIR COMMAND/XPFS
OFFUTT AFB, NB 68113
01CY ATTN ADWATE MAJ BRUCE BAUER
01CY ATTN NRT
01CY ATTN DOK CHIEF SCIENTIST

SAMSO/SK
P.O. BOX 92960
WORLDWAY POSTAL CENTER
LOS ANGELES, CA 90009
01CY ATTN SKA (SPACE COMM SYSTEMS)
M. CLAVIN

SAMSO/MN
NORTON AFB, CA 92409
(MINUTEMAN)
01CY ATTN MNNL

COMMANDER
ROME AIR DEVELOPMENT CENTER, AFSC
HANSCOM AFB, MA 01731
01CY ATTN EEP A. LORENTZEN

DEPARTMENT OF ENERGY
LIBRARY ROOM G-042
WASHINGTON, D.C. 20545
01CY ATTN DOC CON FOR A. LABOWITZ

DEPARTMENT OF ENERGY
ALBUQUERQUE OPERATIONS OFFICE
P.O. BOX 5400
ALBUQUERQUE, NM 87115
01CY ATTN DOC CON FOR D. SHERWOOD

EG&G, INC.
LOS ALAMOS DIVISION
P.O. BOX 809
LOS ALAMOS, NM 85544
01CY ATTN DOC CON FOR J. BREEDLOVE

UNIVERSITY OF CALIFORNIA
LAWRENCE LIVERMORE LABORATORY
P.O. BOX 808
LIVERMORE, CA 94550
01CY ATTN DOC CON FOR TECH INFO
DEPT
01CY ATTN DOC CON FOR L-389 R. OTT
01CY ATTN DOC CON FOR L-31 R. HAGER

LOS ALAMOS NATIONAL LABORATORY
P.O. BOX 1663
LOS ALAMOS, NM 87545
01CY ATTN DOC CON FOR J. WOLCOTT
01CY ATTN DOC CON FOR R.F. TASCHEK
01CY ATTN DOC CON FOR E. JONES
01CY ATTN DOC CON FOR J. MALIK
01CY ATTN DOC CON FOR R. JEFFRIES
01CY ATTN DOC CON FOR J. ZINN
01CY ATTN DOC CON FOR P. KEATON
01CY ATTN DOC CON FOR D. WESTERVELT
01CY ATTN D. SAPPENFIELD

SANDIA LABORATORIES
P.O. BOX 5800
ALBUQUERQUE, NM 87115
01CY ATTN DOC CON FOR W. BROWN
01CY ATTN DOC CON FOR A.
THORNBROUGH
01CY ATTN DOC CON FOR T. WRIGHT
01CY ATTN DOC CON FOR D. DAHLGREN
01CY ATTN DOC CON FOR 3141
01CY ATTN DOC CON FOR SPACE PROJECT
DIV

SANDIA LABORATORIES
LIVERMORE LABORATORY
P.O. BOX 969
LIVERMORE, CA 94550
01CY ATTN DOC CON FOR B. MURPHEY
01CY ATTN DOC CON FOR T. COOK

OFFICE OF MILITARY APPLICATION
DEPARTMENT OF ENERGY
WASHINGTON, D.C. 20545
01CY ATTN DOC CON DR. YO SONG

OTHER GOVERNMENT

INSTITUTE FOR TELECOM SCIENCES
NATIONAL TELECOMMUNICATIONS & INFO ADMIN
BOULDER, CO 80303
01CY ATTN A. JEAN (UNCLASS ONLY)
01CY ATTN W. UTLAUT
01CY ATTN D. CROMBIE
01CY ATTN L. BERRY

NATIONAL OCEANIC & ATMOSPHERIC ADMIN
ENVIRONMENTAL RESEARCH LABORATORIES
DEPARTMENT OF COMMERCE
BOULDER, CO 80302
01CY ATTN R. GRUBB
01CY ATTN AERONOMY LAB G. REID

DEPARTMENT OF DEFENSE CONTRACTORS

AEROSPACE CORPORATION
P.O. BOX 92957
LOS ANGELES, CA 90009
01CY ATTN I. GARFUNKEL
01CY ATTN T. SALMI
01CY ATTN V. JOSEPHSON
01CY ATTN S. BOWER
01CY ATTN D. OLSEN

ANALYTICAL SYSTEMS ENGINEERING CORP
5 OLD CONCORD ROAD
BURLINGTON, MA 01803
01CY ATTN RADIO SCIENCES

AUSTIN RESEARCH ASSOC., INC.
1901 RUTLAND DRIVE
AUSTIN, TX 78758
01CY ATTN L. SLOAN
01CY ATTN R. THOMPSON

BERKELEY RESEARCH ASSOCIATES, INC.
P.O. BOX 983
BERKELEY, CA 94701
01CY ATTN J. WORKMAN
01CY ATTN C. PRETTIE
01CY ATTN S. BRECHT

BOEING COMPANY, THE
P.O. BOX 3707
SEATTLE, WA 98124
01CY ATTN G. KEISTER
01CY ATTN D. MURRAY
01CY ATTN G. HALL
01CY ATTN J. KENNEY

CHARLES STARK DRAPER LABORATORY, INC.
555 TECHNOLOGY SQUARE
CAMBRIDGE, MA 02139
01CY ATTN D.B. COX
01CY ATTN J.P. GILMORE

COMSAT LABORATORIES
LINTHICUM ROAD
CLARKSBURG, MD 20734
01CY ATTN G. HYDE

CORNELL UNIVERSITY
DEPARTMENT OF ELECTRICAL ENGINEERING
ITHACA, NY 14850
01CY ATTN D.T. FARLEY, JR.

ELECTROSPACE SYSTEMS, INC.
BOX 1359
RICHARDSON, TX 75080
01CY ATTN H. LOGSTON
01CY ATTN SECURITY (PAUL PHILLIPS)

EOS TECHNOLOGIES, INC.
606 Wilshire Blvd.
Santa Monica, Calif 90401
01CY ATTN C.B. GABBARD
01CY ATTN R. LELEVIER

ESL, INC.
495 JAVA DRIVE
SUNNYVALE, CA 94086
01CY ATTN J. ROBERTS
01CY ATTN JAMES MARSHALL

GENERAL ELECTRIC COMPANY
SPACE DIVISION
VALLEY FORGE SPACE CENTER
GODDARD BLVD KING OF PRUSSIA
P.O. BOX 8555
PHILADELPHIA, PA 19101
01CY ATTN M.H. BORTNER
SPACE SCI LAB

GENERAL ELECTRIC COMPANY
P.O. BOX 1122
SYRACUSE, NY 13201
01CY ATTN F. REIBERT

GENERAL ELECTRIC TECH SERVICES CO., INC.
HMES
COURT STREET
SYRACUSE, NY 13201
01CY ATTN G. MILLMAN

GEOPHYSICAL INSTITUTE
UNIVERSITY OF ALASKA
FAIRBANKS, AK 99701
(ALL CLASS ATTN: SECURITY OFFICER)
01CY ATTN T.N. DAVIS (UNCLASS ONLY)
01CY ATTN TECHNICAL LIBRARY
01CY ATTN NEAL BROWN (UNCLASS ONLY)

GTE SYLVANIA, INC.
ELECTRONICS SYSTEMS GRP-EASTERN DIV
77 A STREET
NEEDHAM, MA 02194
01CY ATTN DICK STEINHOF

HSS, INC.
2 ALFRED CIRCLE
BEDFORD, MA 01730
01CY ATTN DONALD HANSEN

ILLINOIS, UNIVERSITY OF
107 COBLE HALL
150 DAVENPORT HOUSE
CHAMPAIGN, IL 61820
(ALL CORRES ATTN DAN MCCLELLAND)
01CY ATTN K. YEH

INSTITUTE FOR DEFENSE ANALYSES
1801 NO. BEAUREGARD STREET
ALEXANDRIA, VA 22311
01CY ATTN J.M. AEIN
01CY ATTN ERNEST BAUER
01CY ATTN HANS WOLFARD
01CY ATTN JOEL BENGSTON

INTL TEL & TELEGRAPH CORPORATION
500 WASHINGTON AVENUE
NUTLEY, NJ 07110
01CY ATTN TECHNICAL LIBRARY

JAYCOR
11011 TORREYANA ROAD
P.O. BOX 85154
SAN DIEGO, CA 92138
01CY ATTN J.L. SPERLING

JOHNS HOPKINS UNIVERSITY
APPLIED PHYSICS LABORATORY
JOHNS HOPKINS ROAD
LAUREL, MD 20810
01CY ATTN DOCUMENT LIBRARIAN
01CY ATTN THOMAS POTEMRA
01CY ATTN JOHN DASSOULAS

KAMAN SCIENCES CORP
P.O. BOX 7463
COLORADO SPRINGS, CO 80933
01CY ATTN T. MEAGHER

KAMAN TEMPO-CENTER FOR ADVANCED STUDIES
816 STATE STREET (P.O DRAWER QQ)
SANTA BARBARA, CA 93102
01CY ATTN DASIAC
01CY ATTN WARREN S. KNAPP
01CY ATTN WILLIAM MCNAMARA
01CY ATTN B. GAMBILL

LINKABIT CORP
10453 ROSELLE
SAN DIEGO, CA 92121
01CY ATTN IRWIN JACOBS

LOCKHEED MISSILES & SPACE CO., INC
P.O. BOX 504
SUNNYVALE, CA 94088
01CY ATTN DEPT 60-12
01CY ATTN D.R. CHURCHILL

LOCKHEED MISSILES & SPACE CO., INC.
3251 HANOVER STREET
PALO ALTO, CA 94304
01CY ATTN MARTIN WALT DEPT 52-12
01CY ATTN W.L. IMHOF DEPT 52-12
01CY ATTN RICHARD G. JOHNSON, DEPT 52-12
01CY ATTN J.B. CLADIS DEPT 52-12

MARTIN MARIETTA CORP
ORLANDO DIVISION
P.O. BOX 5837
ORLANDO, FL 32805
01CY ATTN R. HEFFNER

M.I.T. LINCOLN LABORATORY
P.O. BOX 73
LEXINGTON, MA 02173
01CY ATTN DAVID M. TOWLE
01CY ATTN L. LOUGHLIN
01CY ATTN D. CLARK

MCDONNEL DOUGLAS CORPORATION
5301 BOLSA AVENUE
HUNTINGTON BEACH, CA 92647
01CY ATTN N. HARRIS
01CY ATTN J. MOULE
01CY ATTN GEORGE MROZ
01CY ATTN W. OLSON
01CY ATTN R.W. HALPRIN
01CY ATTN TECHNICAL LIBRARY SERVICES

MISSION RESEARCH CORPORATION
735 STATE STREET
SANTA BARBARA, CA 93101
01CY ATTN P. FISCHER
01CY ATTN W.F. CREVIER
01CY ATTN STEVEN L. GUTSCHE
01CY ATTN R. BOGUSCH
01CY ATTN R. HENDRICK
01CY ATTN RALPH KILB
01CY ATTN DAVE SOWLE
01CY ATTN F. FAJEN
01CY ATTN M. SCHEIBE
01CY ATTN CONRAD L. LONGMIRE
01CY ATTN B. WHITE
01CY ATTN R. STAGAT

MISSION RESEARCH CORP.
1720 RANDOLPH ROAD, S.E.
ALBUQUERQUE, NEW MEXICO 87106
01CY R. STELLINGWERF
01CY M. ALME
01CY L. WRIGHT

MITRE CORPORATION, THE
P.O. BOX 208
BEDFORD, MA 01730
01CY ATTN JOHN MORGANSTERN
01CY ATTN G. HARDING
01CY ATTN C.E. CALLAHAN

MITRE CORP
WESTGATE RESEARCH PARK
1820 DOLLY MADISON BLVD
MCLEAN, VA 22101
01CY ATTN W. HALL
01CY ATTN W. FOSTER

PACIFIC-SIERRA RESEARCH CORP
12340 SANTA MONICA BLVD.
LOS ANGELES, CA 90025
01CY ATTN E.C. FIELD, JR.

PENNSYLVANIA STATE UNIVERSITY
IONOSPHERE RESEARCH LAB
318 ELECTRICAL ENGINEERING EAST
UNIVERSITY PARK, PA 16802
(NO CLASS TO THIS ADDRESS)
01CY ATTN IONOSPHERIC RESEARCH LAB

PHOTOMETRICS, INC.
4 ARROW DRIVE
WOBURN, MA 01801
01CY ATTN IRVING L. KOFSKY

PHYSICAL DYNAMICS, INC.
P.O. BOX 3027
BELLEVUE, WA 98009
01CY ATTN E.J. FREMOUW

PHYSICAL DYNAMICS, INC.
P.O. BOX 10367
OAKLAND, CA 94610
ATTN A. THOMSON

R & D ASSOCIATES
P.O. BOX 9695
MARINA DEL REY, CA 90291
01CY ATTN FORREST GILMORE
01CY ATTN WILLIAM B. WRIGHT, JR.
01CY ATTN WILLIAM J. KARZAS
01CY ATTN H. ORY
01CY ATTN C. MACDONALD
01CY ATTN R. TURCO
01CY ATTN L. DeRAND
01CY ATTN W. TSAI

RAND CORPORATION, THE
1700 MAIN STREET
SANTA MONICA, CA 90406
01CY ATTN CULLEN CRAIN
01CY ATTN ED BEDROZIAN

RAYTHEON CO.
528 BOSTON POST ROAD
SUDBURY, MA 01776
01CY ATTN BARBARA ADAMS

RIVERSIDE RESEARCH INSTITUTE
330 WEST 42nd STREET
NEW YORK, NY 10036
01CY ATTN VINCE TRAPANI

SCIENCE APPLICATIONS, INC.
1150 PROSPECT PLAZA
LA JOLLA, CA 92037
01CY ATTN LEWIS M. LINSON
01CY ATTN DANIEL A. HAMLIN
01CY ATTN E. FRIEMAN
01CY ATTN E.A. STRAKER
01CY ATTN CURTIS A. SMITH

SCIENCE APPLICATIONS, INC
1710 GOODRIDGE DR.
MCLEAN, VA 22102
01CY J. COCKAYNE
01CY E. HYMAN

SRI INTERNATIONAL
333 RAVENSWOOD AVENUE
MENLO PARK, CA 94025
01CY ATTN J. CASPER
01CY ATTN DONALD NEILSON
01CY ATTN ALAN BURNS
01CY ATTN G. SMITH
01CY ATTN R. TSUNODA
01CY ATTN DAVID A. JOHNSON
01CY ATTN WALTER G. CHESNUT
01CY ATTN CHARLES L. RINO
01CY ATTN WALTER JAYE
01CY ATTN J. VICKREY
01CY ATTN RAY L. LEADABRAND
01CY ATTN G. CARPENTER
01CY ATTN G. PRICE
01CY ATTN R. LIVINGSTON
01CY ATTN V. GONZALES
01CY ATTN D. MCDANIEL

TECHNOLOGY INTERNATIONAL CORP
75 WIGGINS AVENUE
BEDFORD, MA 01730
01CY ATTN W.P. BOQUIST

TOYON RESEARCH CO.
P.O. Box 6890
SANTA BARBARA, CA 93111
01CY ATTN JOHN ISE, JR.
01CY ATTN JOEL GARBARINO

TRW DEFENSE & SPACE SYS GROUP
ONE SPACE PARK
REDONDO BEACH, CA 90278
01CY ATTN R. K. PLEBUCH
01CY ATTN S. ALTSCHULER
01CY ATTN D. DEE
01CY ATTN D/ STOCKWELL
SNTF/1575

VISIDYNE
SOUTH BEDFORD STREET
BURLINGTON, MASS 01803
01CY ATTN W. REIDY
01CY ATTN J. CARPENTER
01CY ATTN C. HUMPHREY

UNIVERSITY OF PITTSBURGH
PITTSBURGH, PA 15213
01CY ATTN: N. ZABUSKY

DIRECTOR OF RESEARCH
U.S. NAVAL ACADEMY
ANNAPOLIS, MD
02CY

END

FILMED

7-85

DTIC